COMPUTATION OF THE PROPERTIES OF ORGANIC-INORGANIC TIN HALIDE PEROVSKITE FOR PHOTOVOLTAIC APPLICATION; FIRST PRINCIPLES APPROACH

PERPETUA JELIMO CHEMAOI

A Thesis submitted to the Institute of Postgraduate Studies of Kabarak University in Partial Fulfillment of the Requirements for the Award of Master of Science in Physics Degree.

KABARAK UNIVERSITY

NOVEMBER 2022

DECLARATION

1. I do declare that:

   i.   This thesis is my own work and to the best of my knowledge, it has not been presented for the award of a degree in any university or college.

   ii.   The work has not in-cooperated material from other works or a paraphrase of such material without due and appropriate acknowledgement.

   iii.   The work has been subjected to processes of anti-plagiarism and has met Kabarak University   15% similarity index threshold.

2. I do understand that issues of academic integrity are paramount and therefore I may be suspended or expelled from the University or my degree may be recalled for academic dishonesty or any other related academic malpractices.

PERPETUA JELIMO CHEMAOI

REG. NO: GMP/M/0282/04/18

Signature: …………………………..   **Date**: ……………………………..

RECOMMENDATIONS

To the Institute of Postgraduate Studies:

This thesis entitled "**Computation of the Properties of Organic-Inorganic Tin Halide Perovskites for Photovoltaic Application; First Principles Approach**" written by **Perpetua Jelimo Chemaoi** is presented to the Institute of Postgraduate Studies of Kabarak University. We have reviewed the thesis and recommend it to be accepted in partial fulfillment of the requirements for the award of Master of Science in Physics.

Signature: ………………………..   **Date**: ……………………………..

Dr. Phillip Otieno Nyawere

Department of Biological & Physical Sciences,

Kabarak University.

Signature: …………………………..   **Date**: ……………………………..

Prof. Christopher Maghanga

Department of Biological & Physical Sciences,

Kabarak University

entire church, especially my students of the A.I.C Christian Wife's Fellowship, everything is possible in the hands of our Almighty God.

Finally, I thank the Center for High-Performance Computing (CHPC) which is in Cape Town, South Africa for providing a High Performance Computing facility that was used in all the calculations in this thesis. Also my appreciation goes to Materials Science and Solar Energy Network for Eastern and Southern Africa (MSSESA), US-Africa Initiative in Electronic Structure and the Computational and Theoretical Physics (CTheP) for constantly providing me with the platforms to present my work, networking with other researchers and workshops they organized that gave a wider understanding of DFT and the quantum espresso software that greatly helped me in my research.

DEDICATION

This work is dedicated to my children; Elsa Jepkoech**,** Lelys Jeptoo and Agustus Kipkosgei.

ABSTRACT

The energy demand in today's society is ever increasing because of the continuous increase in population. Solar energy that uses solar cells which converts solar radiation to electrical energy is of great importance. The first and second generation solar cells in use are made of silicon that involves high cost of fabrication and lack of longevity of the electric power generated. Therefore research has shifted to perovskite based solar cells which have proven to be novel candidates for photovoltaic application because of their availability and low cost of fabrication. However, they have not been commercialized for photovoltaic applications because of their short life times which is around one year. The purpose of this research was to study the electronic, structural, the elastic and the dielectric properties of DASnI3 with an increased stability and the materials' potential photovoltaic application. Therefore in this work first principle calculation and modeling based on Density Functional Theory (DFT) implemented in Quantum espresso was used. The electronic, structural, elastic and the dielectric constants of dimethylammonium triiodostanate(II) were determined using density-functional theory within generalized gradient approximation (GGA) using plane-wave basis set pseudopotentials method and using the Voigt–Reuss–Hill averaging scheme for Elastic constant parameters. From this study lattice parameter a, b and c as 8.505 Å, 9.232 Å and 15.040 Å were obtained respectively for an orthorhombic DASNI3 with 60 atoms. The band gap of 2.7ev and the Poisson's ratio (v) of 0.36 were obtained from this work. Dielectric constants which include the real (ε_1) and imaginary part (ε_2) and the absorption coefficient were calculated the absorption begun from 2.5eV. The anisotropy of 1.7 was also obtained. The values obtained for all the parameters were compared with the available experimental and theoretical values. It was observed that there was a fairly good agreement from the studies with this computational work. It was concluded that this material is suitable for photovoltaic application. These findings can be used to test experimentally the use of DASnI3 perovskite in solar cells.

Key words: Photovoltaic, First Principle, Density Functional Theory, Perovskite.

TABLE OF CONTENTS

LIST OF FIGURES

LIST OF TABLES

LIST OF ABBREVIATIONS AND ACRONYMS

Br   Bromine

CaTiO₃   Calcium Titanate

Cl   Chlorine

DASnI3   Dimethyl Ammonium Tri-iodostanateII

DFT   Density Functional Theory

DOS   Density of State

D$_r$ Intrinsic Diode

e   Electronic Charge

Eg   Band Gap

ETM   Electron Transmitting Media

Espresso opEn Sources Package for Research in Electronic Structure Simulation and optimization.

FA   Formamidinium (NH_2-CH-NH_2)

FPAPW   Full Potential Augmented Plane Wave

GGA   Generalized Gradient Approximation

H   Total Hamiltonian

HOMO   Highest Occupied Molecular Orbitals

HPSCs   Hybrid Perovskite Solar Cells

HTM   Hole Transmitting Media

I   Iodine

J$_{PH}$ Photon Induced Current

KS   Kohn Sham

LAPW   Linearized Augmented Plane Wave

LUMO   Lowest Unoccupied Molecular Orbitals

m	Electron Mass
MAPbI₃	Methylammonium Lead Iodide ($CH_3NH_3PbI_3$)
MASnI₃	Methylammonium Tin Iodide ($CH_3NH_3SnI_3$)
PAW	Projected Augmented Wave
Pb	Lead
PBE	Perdew Burke Ernzerhof
PL	Photoluminescence
PCE	Power Conversion Efficiency
PDOS	Partial Density of States
PIN	Positive Intrinsic Negative
QE	Quantum Espresso
$\bar{R}_1$	Nuclei Positions
sc-Si	Single Crystalline Silicon
scf	Self-Consistent Field
Sn	Tin
2D	Two Dimensional
3D	Three Dimensional

OPERATIONAL DEFINITION OF TERMS

Band Gap: This is the distance between the valence band maximum of electrons and the conduction band minimum. It can also be defined as the difference in energy between the valence band and the conduction band of a solid material for an insulator or a semiconductor and consists of the range of energy values that are forbidden to electrons in the material.

Electronic Properties: These are parameters and representations that describe the state and the behavior of electrons in a material

Optical Properties: This is the material response to incident radiation and it is described as reflectance, absorption, refraction and transmittance

Mechanical Properties: These are the physical properties exhibited by a material upon application of forces. These properties include the tensile strength, modulus of elasticity and elongation.

Photoelectric Effect: This is a phenomenon in which electrically charged particles are released from or within the material when light falls on it.

Photoelectron: This is an electron emitted from an atom by an interaction with a photon, especially by the action of light.

Photoluminescence: This is when light energy or photons stimulate the emission of a photon which can be in the form of fluorescence that excites a molecule raising it to an electronic excited state.

Photovoltaics (PV): This is the conversion of light into electricity by use of semiconducting materials that exhibit the photovoltaic effect.

Perovskite: It is a name applied to the class of compounds that exhibit the same type of crystal structure as $CaTiO_3$

Solar Cell: This is an electrical device that converts the light energy directly to electricity through photovoltaic effect.

Young's Modulus: This is a property of the material that tells us how easily it can stretch and deform and is defined as the ratio of tensile stress (amount of force applied per unit area) to tensile strain (extension per unit length)

Bulk Modulus: This is the relative change in volume of a body produced by a unit compressive or tensile stress acting uniformly over the surface.

Shear Modulus (G): It is the measure of the elastic shear stiffness of a material and is defined as the ratio of shear stress to the shear strain.

Anisotropy Factor (E): This is the average of the cosine of the scattering angle θ and has a probability density with a single scattering direction as a parameter.

CHAPTER ONE

INTRODUCTION

1.1 Introduction

This section discusses the background of the concepts on perovskites and problems to be addressed towards application of organic-inorganic tin halide perovskites in photovoltaics. It further proceeds to state the research problem, outlining the objectives, lists the research questions, defines the significance, scope and the assumptions of the study.

1.2 Background of the Study

The demand for energy in today's society is growing continuously due to the ever-increasing population. The conventional use of nonrenewable energy sources which include gas, petroleum and coal, are becoming limited and environmentally unfriendly due to pollution. The adverse climate change due to the changing weather patterns causes low water levels to pose a threat on hydro-generation. The search for a reliable and viable source of energy is ongoing. Solar energy is one of the most promising of all the forms of energy available. This is because of its abundance and it is also a clean renewable form of energy. At present, Silicon solar cells are widely used among all solar cells due to their high efficiency in terms of single crystalline cell photovoltaic devices. According to White *et al.,* (2013) the efficiency of single crystalline (sc-Si) is heading towards above 30%. However, high cost of fabrication is involved in making single crystalline silicon (sc-Si) according to Wong *et al.,* (2016), which has increased recent research interests for the next generation of thin film solar cells with the aim of finding a solar cell cheaper than silicon.

Recently, the development of perovskite-based solar cells have rapidly passed the efficiencies of many emerging, commercial photovoltaics such as dye-sensitized and amorphous silicon solar cells (Giannouli *et al*., 2021). Perovskite is a term given to all compounds which have the general chemical formula ABX_3 and the crystal structure of calcium titanate $CaTiO_3$. They are Organic-inorganic metal halide perovskites, where *A* is an organic cation, *B* being a divalent metal ion, and *X* is a halide such as $CH_3NH_3Pb_3$ (Methylammonium lead halide). They are promising alternatives to silicon, because they are cheap and are abundant starting materials according to Cheng *et al.,* (2010) and can be manufactured by simple solution processing.

The interest in the study of these organic-inorganic hybrid perovskite materials has been largely inspired by the interesting characteristics of the inorganic components, such as their thermal stability and their high degree of structural order (Fan *et al.,* 2014). Also, other motivating interests are the properties of the organic components which include their functional versatility, their mechanical flexibility and are at low-cost of processing (Gianelis, 1996).

Solar cells that are based on hybrid organic-inorganic lead-halide perovskites have significantly risen in efficiency in recent years. Lead is toxic and thus the primary challenge with this material and the key concern is to replace lead in the perovskite crystal with a less toxic metal. This has resulted in the need for the search of related compounds that may replicate the properties of the hybrid lead-halide perovskites which are tolerant to defects and have long lifetimes.

The most likely and viable replacements of lead in the perovskite material are Tin and Germanium because they are also members of group 14 metals in the periodic table. Tin is closely analogous in many aspects to lead such as their ionic radii. The ionic

radius for lead is 1.49 Å, tin 1.35 Å while Germanium is 0.3 Å. Tin can therefore substitute lead with insignificant perturbation. However, it is known that the stability of the 2^+ oxidation state when moving up the group 14 elements decreases, this being the major problem in the use of these metals and hence their chemical instability in the required oxidation state as argued by Babayigit et al., (2016). Appropriate materials for photovoltaic application in an efficient solar energy conversion are expected to have a suitable energy band gap in the visible range of electromagnetic spectrum, the high absorption coefficient of sunlight and according to Zhou et al., (2018) the material should exhibit high mobility of electrons and holes and also a high ability of transforming solar energy into electrical energy.

A study done by Ke et al., (2018) on the use of the dimethylammonium iodide (DAI) and related compounds stabilizes the perovskite phase. This is achieved due to the effect on the lattice geometry when DA is used. This alters the size and the tilting of the BX6 octahedra. The degree of the tilt affects band gap by increasing the octahedral tilt decreasing the level of the overlap between metal and halide orbitals thus pushing the valence band further from the vacuum Eperon et al., (2020). Incorporating DAI into the perovskite solar cells can improve both air, thermal stability and the charge transport property Pisanu et al., (2019) and Bian et al., (2020).

First principle computation is a quantum mechanical method aiming at solving the electronic Schrödinger equation with the knowledge of the nuclei positions and the number of electrons in the system. This is a numerical simulation method which is necessary in order to explore most of the properties which include structural, electronic, transport, magnetic, mechanical and physical properties. The studies by Babkin et al.,

(2011), points out that band structure calculations is an effective theoretical tool for researchers to predict such properties.

Density functional theory (DFT) is a theory that correlates many body systems used in computational physics or chemistry to analyze the structural, electronic and magnetic properties of materials at ground state under pressure or with variation of temperature using first principle study. DFT, is a scientific approach of finding solutions to the Schrödinger equation that describes the quantum behavior of atoms and molecules having in mind the practical values. Thus, DFT is a legitimate method of theoretical predictions to describe the properties of a collection of atoms. DFT through first principle calculations can also be used to search for similar reactions that occur at pressures accessible experimentally as shown by Feliciano (2014). Hence first principles calculation based on DFT was used to determine the structural, electronic, optical and elastic properties of DASnI3.

1.3 Statement of the Research Problem

Tin based perovskites have not been commercialized in thin film technology for photovoltaic applications this is because of the perovskite's short life time which is approximated to be about one year (Songvilay *et al*., 2019). Thus the great interest of this research was to improve the atomistic understanding of the structural, electronic, optical and elastic effects of DASnI3 having a longer A-cation on the polarization effects and the hydrogen bond formation. The interaction of the organic A-cation, with the iodine migration and lattice distortion could influence the stability of the material (Grancini, *et al;* 2017). The stability of Tin based perovskite could be improved by optimizing the band gap, increasing the light harvesting efficiency and other issues like enlarging the cell size where scalable production can be realized thus accelerating the commercialization of the tin perovskites solar cells. The certified efficiency of tin based

perovskite at the accredited test center is 11.22% which is lower than lead-based solar cells whose reported highest efficiency is 25.5% and is comparable to the silicon solar cell (Wu *et al.*, 2021). Therefore, this research explored the properties of tin halide perovskites with a view of studying the applicability of DASnI3 perovskite solar based cell. Computational modeling was employed where simulations of the properties of tin-halide perovskite solar cells were studied for its applicability in solar cells and generally for photovoltaic applications.

1.4 Objectives of the Study

The main objective of this study was to determine the structural, electronic, dielectric and elastic properties of Dimethyl ammonium triidostanate II (DASnI3) a tin halide perovskites by first principle calculation for photovoltaic application.

Specific Objectives

i. To determine the structure of DASnI3 by first principle.

ii. To determine the electronic properties of DASnI3 for photovoltaic application by first principle.

iii. To study the dielectric constants of DASnI3 and their photovoltaic application by first principles.

iv. To compute the elastic constants of DASnI3 by first principles and establish its photovoltaic application.

1.5 Research Questions.

The research seeks to give answers to the following questions: -

i. What is the structure of DASnI3 obtained using first principle?

ii. What are the electronic properties of DASnI3 by first principles and how do they compare with other works?

iii. Which dielectric constants were obtained by first principles for DASnI3 and how do they compare with results from other studies.

iv. How are the elastic constants properties obtained for DASnI3 by first principles compare with those obtained from other studies and their application in photovoltaics?

1.6 Significance of the Study

Numerical simulation technique is a viable tool which has over the years proven to be used in studying and understanding the properties of solar cell devices. Some of them include the study of optical, electronic and mechanical properties of materials which are complex and are used in solar cell devices according to Burgelman *et al.,* (2004). The study helps in providing useful information to reduce the cost of processing and time spent on fabrication of solar cell devices by stating the production parameters and hence improvement of the performance of the device (Minemoto *et al.,* 2014).

1.7 Justification of the Study

Measurements and calculations of the basic properties which include the crystal structure, the electronic structure and even material composition, can be challenging .This is because some of these materials have anisotropic structures, while others can be composed of mobile and light elements. These can be beam damaged when characterizing or change of composition in vacuum state or even compound defects such as the alterations of the electronic structures because of the substrate influence. This makes it a challenge in understanding the basic properties in their operation. All these effects compounded have made their study difficult and hence created a need to continuously evaluate the best practices of characterizing and calculating material properties.

The laws of quantum mechanics govern the interaction between atoms and electrons. The analysis of quantum mechanical equations is required to solve the basic quantum mechanical equations using Density Functional Theory (DFT). DFT has been successful in determining quantum mechanical properties of materials at ground state.

From the study, it is shown that tin halide perovskite can be used in solar cells fabrication. The results obtained from this study should therefore supplement the experimental fabrication of tin halide perovskites to be used in solar cells. It is further expected that the results of the study will add to the body of knowledge in respect to tin halide perovskites.

1.8 Scope of the Study

This study focused on structural, electronic, dielectric and elastic properties of Dimethyl ammonium triiodostanate II perovskites .The findings will be used determine the photovoltaic application of organic-inorganic tin halide perovskites. Computational modeling methods based on Density Functional Theory were used and may not apply to other perovskites. Quantum Espresso was used in the study of all the properties with GGA+U in Optical properties and Thermo_pw for Elastic Properties.

1.9 Assumptions

The assumptions made were:

i. The quantum espresso code used, would effectively carry out quantum analysis and could be used to determine the desired properties despite the associated shortcomings of the code.

ii. The data and information on the properties of Dimethyl ammonium triiodostanate II and other similar works would be available.

iii. The time to carry out the research would be sufficient to come up with the desired findings that would give answers to the stated objectives.

CHAPTER TWO

LITERATURE REVIEW

2.1 Introduction

This chapter discusses the properties of organic-inorganic tin halide perovskites that are relevant to their applications in photovoltaics. Literature on structural and electronic properties, mechanical, optical and the study of power conversion efficiency will be discussed. The prototype conceptual framework will also be presented and discussed.

2.2 Perovskite Solar Cell

To develop photovoltaic systems that are cost-effective and are alternatives to silicon solar cells, solar cells based on perovskites have attracted considerable interest according to Snaith *et al.,* (2014). Some of the solar cells used currently include dye-sensitized, organic, and amorphous silicon solar cells (Green *et al.,* 2014).

A perovskite is any material with crystal structure same as calcium titanium oxide $CaTiO_3$ with a formula ABX_3. Where *A* is an organic cation, example are the methylammonium MA (CH_3NH_3) or formamidinium FA ($NH_2-CH-NH_2$) , *B* a divalent metal ion and *X*, represents halogens which can be fluoride(F^-) Chloride(Cl^-), Bromide (Br^-) or Iodide (I^-) ions according to Chen, *et al.,* (2015). Also, in the ABX_3 structure, *A* is usually larger in size than *B* (Green *et al*., 2014). The perovskites structure currently used in solar cell devices has a network of BX_6 octahedral corner-sharing, the *B* cation typically Sn^{2+} or Pb^{2+} and *X* being the halogen. Some of the materials properties in which the halide perovskites possess that are of interest for optical sources include bright photoluminescence, tunable exciton binding energy, narrow light emission line width and balanced charge-carrier mobility (Stranks *et al.,* (2013), Sutherland & Sargent, (2016)). The perovskite occupies different phase symmetries, highest being

the Pm3m space group according to Quan *et al*., (2019). Where the ions are perfectly packed, and their ionic radii is given by;

$$r_A + r_X = \sqrt{2(r_B + r_X)} \qquad \qquad \text{… (2.1)}$$

Where the ionic radii of *A*, *B*, and *X* are given by r_A, r_B and r_X. A tolerance factor given by *t* and an octahedral factor denoted by μ was proposed by Goldschmidt for the study of the stability of perovskites. The factor *t* is used to indicate the state of distortion

which is given by $\qquad t = \dfrac{r_A + r_X}{\sqrt{2(r_B + r_X)}} \qquad \qquad \text{… (2.2)}$

Goldschmidt further stated that the octahedral factor is given by the ratio of $\dfrac{r_B}{r_X}$ for the case of the BX_6 octahedron. Generally, hybrid perovskites present an octahedral factor which lies between *0.44* and *0.90* and tolerance factor lying between 0.81 and 1.11. For perovskites with the cubic structure tolerance factor *t* range 0.9 - 1.0, whereas the range exhibited by the tetragonal and the orthorhombic structures is between 0.71 and 0.90 Quan *et al*., (2019), and Lekina & Shen, (2019).

2.3 Structural and Electronic Properties of Perovskite Materials

Perovskite materials which are organic-inorganic in nature are widely used as photo-absorbers in perovskite based solar cells. The interesting characteristics of their inorganic components in the organic-inorganic hybrid perovskite materials include good thermal stability and their high degree of structural order Fan *et al*., (2014) and also due to the properties of the organic component which include their functional versatility, low processability cost and are mechanically flexible (Giannelis, 1996). Hence, the possibility in the merging of the properties of typical inorganic crystals and

those of molecular organic solids has stimulated recent research into versatile properties of hybrid perovskite materials which are organic-inorganic in nature.

 The 3-dimensional perovskite-like structures are formed if the *A, B* and *X* ions fit the ratio determined by the Goldschmidt tolerance factor *t* in Equation *2.2* above. The Goldschmidt Tolerance Factor according to Cheng *et al*., (2010), strictly limits the radius of the cation *A*. *MASnI$_3$* perovskite just like the MAPbI$_3$ possesses a tetragonal crystal structure but only under different temperatures according to Stoumpos *et al*., (2013). It has the lattice parameters of *a* = 8.7912 Å and *c* = 4.4770 Å. Incorporating MA does not necessarily reduce the formation of defects but incorporating the dipolar MA cation with mixed cation mixed halide will not only widen the band gap of the perovskites but it also heals deep trap defects which results in to a more defect-tolerant material (Tan *et al*., 2018). For an ideal cubic halide perovskite the B-site which is the divalent metal will be located at the body-centered position of the cube, while the anions will occupy the six face-centered locations which forms an octahedral surrounding for the divalent metal, while the monovalent cations are situated at the vertices of the cube.as shown in figure 1.

Figure 1:

The Orthorhombic Phase of CH₃NH₃SnI₃ Represented as Balls and Sticks in (a) and Polyhedral Style (b)
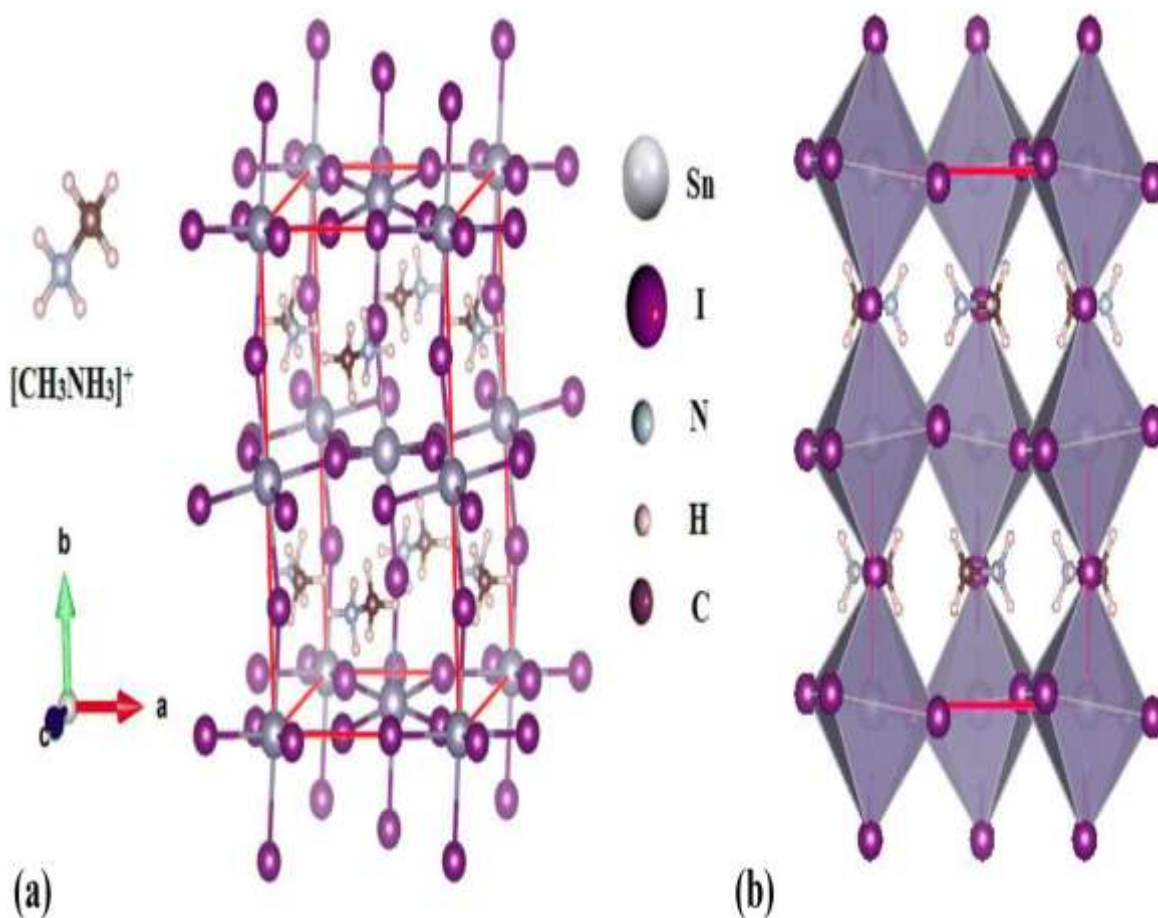
Adapted From Paschal *et al*., (2020).

Apart from the three-dimensional perovskites, there are low dimensional perovskites which exhibit special properties because of their unique structures. These structures have structural freedom due to reduced dimensionality. There is the possibility of creating tunable photo-physical and electronic properties. The Highest Occupied Molecular Orbitals and the lowest Unoccupied Molecular Orbitals energy gap of the organic molecules is usually much higher compared to the band gap of the inorganic layer (Mitzi, 1999). Niemann, *et al.,* (2016) also adds that when the composition is

altered that is going for low dimensional perovskites, it allows tuning of the band gap and also the optical properties of that material efficiently.

A new choice of *A* site cation for instance Formamidinium (FA) which is larger in size than methylammonium (MA), which in turn is larger than Caesium (Cs), results in an increase of band gap going from FA to MA to Cs this is due to the modification of the lattice constant. The extent of metal-halide orbital overlap is influenced by the A-site cation. Philippe, *et al* (2017) states that this change of the bonding of the metal halide has a direct impact on band positions, the valence band and the conduction. For instance, when one uses Formamidinium (HC $(NH_2)_2$), as the A site cation the band gap of the perovskite reduces by about 0.07 eV when compared with MA perovskite. This fact has been exploited to achieve the most recent advances in photovoltaic performances. This shows that FA produces more thermally stable materials and are also promising materials in reaching higher efficiencies in photovoltaics. However, the phase instability exhibited by the $FAPbI_3$ perovskites shows that it is difficult to maintain the desired photoactive black phase at room temperature. This has led to a considerable recent focus on 3D perovskites where the A cation is replaced with Cs+ or Dimethylammonium (DA). The 3D perovskites exhibits have been proven to exhibit a sharp optical absorption onset, according to De Wolf *et al.,* (2014).

Dimethyl Ammonium (DA) is larger in size than methylammonium (MA), resulting in an increase of the band gap (Hautzinger *et al*., 2020). This causes a modification of the lattice constant. The extent of the metal-halide orbital overlap is influenced by the A-site cation. Philippe, *et al* (2017) states that this change of the bonding of the metal halide has a direct impact on band positions, the valence band and the conduction band. For instance, when DA is used as the A site cation the band gap of the perovskite

increases as compared with MA perovskite. This fact can be exploited to achieve the most recent advances in photovoltaic performances. This shows that DA produces more thermally stable materials and are also promising materials in reaching higher efficiencies in photovoltaics (Goetzberger *et al.,* 2003)

The physical and chemical properties of a system are affected by the interaction of electrons with atomic cores. In the cores there are three interactions: the electron-electron interaction, the electron-nuclear interaction and the nuclear-nuclear interaction. The major source of difficulty in these interactions is the treatment of electron-electron interaction while interpreting the properties since the interactions are inseparable and can only be treated with approximation. There are many forms of modeling approaches that are majorly *ab-initio* in nature (Giannozzi *et al.,* 2001). A well solved Schrödinger equation for a specific system can be differentiated from one to another. The solution of these Schrödinger equations remains a difficult task. The exact solutions of these equations, in general, can only be solved if time is exponentially scaling with the system size (Giannozzi *et al.,* 2001). This scaling prevents the exact calculations for all except for the smallest and simplest of systems. The introduction of approximations which are used to reduce the equations to a form that can be solved, reduces the degree of accuracy and the predictive power. Using computer simulation and applying the density functional theory (DFT) methods involved in various solution of the Schrödinger equations has had remarkable success in calculations involving electronic and structural properties and other material properties which are applicable to several other systems . Generally, the DFT among other approaches that involve approximations for the electron-electron interactions have been reported to limit achievable accuracy in their calculations.

2.4 Elastic Properties of Organic-Inorganic Perovskites for Photovoltaic Application

The organic-inorganic halide perovskite materials of the form $CH_3NH_3BX_3$, where B can be *Tin (Sn)* or Lead *Pb* and X can be Iodine, Bromine or Chlorine in solid state sensitized solar cells, as light harvesters from reports shows impressive efficiency values going up to 16% according to Burschka, (2013). The absorbing performance of perovskite solar cells strongly relies on the crystallinity and state of stress on the perovskite thin absorber layer solar cell with different metal cations, the halide species, and the organic cations according to Kim, (2013). To guide the applications of such materials in planar heterojunction solar cells fabricated on flexible polymer substrates, Docampo *et al* (2013) states that first-principles calculations are necessary due to the difficulty in measuring the mechanical properties. According to Bretschneider *et al.* 2014, the mechanical properties of such a perovskite in the system are important in practical applications. The mechanical properties of $CH_3NH_3BX_3$ compounds are used when analyzing the strain, stress, fracture mechanics, and also the deformation of solid, especially the absorber layers in application. The elastic properties are determined by the type and strength of the chemical bond between B and X (Feng, 2014). Furthermore, the B, X and B hinged octahedral allow for wide adjustment which include the bond angle adjustments and several sets of cooperative rotations known as tilt transitions. These promote symmetry, thus showing different structures when the system is at different temperatures. Experimentally, altering the combination of the organic-inorganic components, the organic-inorganic super lattices are obtained quite easily in the starting solution in which the hybrids are crystallized. Thus, the dimensionality can also be used as a further degree of freedom when tuning the material properties of different disordered structures when temperatures are different. An example are the

three phases which exist in *CH₃NH₃BX₃* a compound exhibiting pseudo cubic at high temperature while at medium temperature it exhibits tetragonal structures and at low temperature is the orthorhombic phase. Feng (2014) investigated the elastic constants C_{ij} by the stress-strain method based on the first-principles calculations, and obtained c_{ij} by calculating total energy as a function of the appropriate lattice deformation, and obtained elastic-strain energy by applying the following equation.

$$U = \nabla E/V_o = \frac{1}{2}\sum_i^6\sum_j^6 c_{ij}e_i e_j \qquad \ldots (2.3)$$

Where ΔE is the difference of energy and V_o is the volume of the original cell.

2.5 Optical Properties of Tin Halides

The characteristics of luminescent devices depend on the optical properties resulting from the ion-host interactions. Solar cells that are lead halide based perovskites exhibit high power conversion efficiencies and they are approaching commercialization stage. These perovskites also show unique luminescence properties. According to Kanemitsu and Handa, (2018).Yamada *et al.,* (2017) states that these materials exhibit extremely high photoluminescence (PL) quantum efficiencies at room temperature even when lead halide perovskites are fabricated by simple and inexpensive low temperature solution processing. They further stated that photon recycling of both free-carrier and exciton luminescence were observed in various halide perovskites because of their high PL quantum efficiencies. The high PL quantum efficiency is considered to enable new optical functionality of perovskites as light emitting devices Handa *et al*., (2019). The study of the band gap energy for a semiconductor is necessary for the analysis of optical properties of materials. The bandgap energy is important when considering its application in solar cell devices. According to Shockley, 1961, the bandgap determines

the theoretical upper limit of the cell efficiency through the detailed balance principle, where the bandgap (E_g) depends on the photoluminescence (PL) quantum efficiency of the material used. To achieve an efficient device, it is important to bear in mind that when the optimum PL quantum efficiency becomes smaller than unity, the optimum E_g for the highest possible solar cell efficiency becomes larger. The PL quantum efficiency depends on the recombination dynamics of the photo carriers in the material. For a PL quantum efficiency of 100%, the optimum band gap energy E_g for a single junction solar cell is 1.34 eV under solar illumination AM 1.5G as derived from the detailed balance theory.

A study done by Jelicoe *et.al.* (2016) on synthesis and optical characterization of CsSnX Nano crystal perovskites where X is chlorine, Bromine or iodine, indicated that the band gap adjustment was achieved by tuning the halide composition and spatial confinement. They also indicated that all the species of nanocrystals adopted the perovskites structures. On optical properties they performed transient photoluminescence on solution dispersed particles and observed some spectral shifts. Thus, indicating a likelihood of coming up with good optical properties.

2.6. Photovoltaic Application of Perovskite Solar Cell

In establishing the photovoltaic applicability of perovskite solar cells, Grånäs, *et al.* (2016) investigated the impact of the perovskite structure in the presence of different ions of the A, B and X sites in photovoltaic performance, using electronic structure calculations. Their results showed that the level of alignment of the electron- and hole-transporting media is key to reaching maximum efficiency for heterogeneous (PIN) positive-intrinsic-negative junctions. Low-dimensional perovskite formed by replacing the small hydrophilic cations with much bulkier organic ones can help to improve the stability of the Hybrid Perovskite Solar Cells (HPSCs) upon exposure to moisture. The

preferential crystal orientation and high degree of crystallinity are fundamental for the improvement of solar cell performance. The 2D/3D-based Hybrid Perovskite Solar Cells are highly stable upon exposure to light or ambient conditions. This is due to the enhanced robustness of the perovskite film. The power conversion efficiency of the solar cells based on perovskite is high depending on the chemical composition of the perovskite layer and also the electronic structure properties of the electron and hole transporting media when using the thermodynamic approach as argued by Shockley and Queisser (1961).

2.7 Operational Principle of Perovskite Solar Cells

Some of the enticing properties of Organic-inorganic hybrid perovskite materials that makes them potential for applications in photovoltaic devices include:

First, the light-harvesting characteristics which are excellent and also good hole transporting properties (Liu *et al.,* 2013).

Secondly, the printing techniques that use low temperature solar cell processing make it possible for the deposition on a flexible substrate (Fan *et al*., 2014).

Thirdly, low energy-loss due to increased light absorption increases the photo generation of free charge carriers. This enables the charges to be generated and hence increases the charge collection at the electrodes (Stranks *et al*., 2013)

Lastly, low processing cost with high efficiency which means low energy payback time.

Despite the aforementioned advantages of organic-inorganic hybrid perovskites, there are generally some challenges facing perovskite solar cells, which still hinder their commercialization. Research is still ongoing to address some of these challenges in various capacities. These problems include:

First, lead, which is one of the most used solar cells perovskite, is toxic and leaching could occur into the environment causing health as well as ecological challenges. Hence, environmentally friendly elements such as tin have recently been proposed for solar cell materials alternatives to lead perovskites.

Secondly, perovskite materials are salt-like crystal structures thus are extremely sensitive to water vapor and also oxygen and hence dissolves easily. However, it has been addressed by preparing them in an inert atmosphere according to Mitzi *et al.,* (1995). It is then followed with encapsulation of the whole device within the air-tight sealant in the same inert condition. This is not cost effective for large scale production, however it has been used to reduce the degradation and oxidation of Sn^{2+} to Sn^{4+} which has increased the tin perovskite solar cell lifetime for a period of up to 4-months (Noel *et al.,* 2014).

Lastly, preparing large continuous films in glove boxes is challenging, this limits large scale production of the perovskite solar cells. However, sequential deposition of the constituent's components perovskite materials has been used to get a continuous film over a larger area without degradation of the cell efficiency (Burschka *et al*., 2013)

2.8 Research Gaps

The table below shows the indexing parameters for various properties of materials.

Table 1

A Template Showing the Elastic, Electronic and Optical Parameters of Perovskite Materials.

Property name	Property value	Reference
Band gap	1.34	Martin et *al*, 2020
Poisons Ratio	>0.26	Feng *et al*, 2014
Pugh's ratio (B/G)	1.75	Orio *et al,* 2009
Anisotropy	1	Martin *et al*, 2022
Visible light range	1.6 eV -3.5eV	He *et al*, 2022

The optimum band gap energy E_g for a single junction solar cell is 1.34 eV under solar illumination AM 1.5G for a PL quantufficiency of 100%, as derived from the detailed balance theory. A material is ductile if Pugh's ratio B/G value is higher than 1.75 and the poisons ratio should be greater than 0.26 a material with a lesser value is brittle. The anisotropic parameter (A) for an ideal isotropic system, is unity and diverges from unity for an anisotropic systems. According to He *et al,* (2022), visible light range falls between 1.6eV to 3.5eV therefore a good absorber material should absorb light within this range.

Figure 2 below illustrates the proposed conceptual framework. It has three sets of variables; the dependent, independent, and intervening variables. The independent variables are the material properties which are obtained using the input files, the pseudopotentials and thermo-pw the dependent variable is the photovoltaic application of tin halide perovskite while the software used is the intervening variable. It was hypothesized that the stated variables would influencethe photovoltaic application of

19

tin halide perovskite. This general hypothesis guided this study. The properties were obtained by calculating the total energies, lattice parameters, studying the band arrangement, elastic constants and the absorption efficiencies.

2.9 Conceptual Framework

Figure 2

Conceptual Framework

Independent Variables   **Intervening Variables**   **Dependent Variables**

Structural and Electronic Properties of DASnI3 by first principles.

Dielectric constants of DASnI3 by first principles

Elastic constants of DASnI3 by first principles

Computational codes

Photovoltaic application through the structural, electronic, dielectric and elastic properties of DASnI3

CHAPTER THREE

RESEARCH METHODOLOGY

3.1 Introduction

Computational modeling is the use of computer programs to simulate and study complex systems using a software. It is a scientific research design where the reproduction of the behavior of a system is done. Computer codes are used to simulate the outcomes of a mathematical model associated with the said system. Computational modeling describes the properties of matter rooted on equations. The properties determined include; electronic, optical, and elastic properties of tin halide perovskite, and the photovoltaic applications. Computer simulation is realized by running computer programs implemented in quantum espresso code. Thus, we described how Quantum Espresso operates and derived the mathematical equations solved by the software based on Density Functional Theory. Also, the device structure that carried out the simulation and optimization was described.

3.2 Description of the Working of Quantum Espresso

Quantum espresso is a software suited for first principle calculation and modeling and it is written in Fortran. Espresso is an acronym for opEn Source Package for Research in Electronic Structure, Simulation and Optimization based on Density Functional Theory (DFT), plane wave basis sets, and also on pseudopotentials.

The plane wave DFT functions of QE was provided by the plane-wave self-consistent field (PWscf) which is a set of programs for electronic structure calculation within DFT which uses plane wave basis sets and pseudopotentials.

These PWscf were used to solve the self-consistent scheme of Kohn Sham equations obtained for a periodic solid, to carry out total energy calculation and post processing

21

which allowed data analysis and plotting. Quantum espresso calculates the ground-state energy and one-electron Kohn-Sham orbitals to be able to find atomic forces, stresses, and optimization of structures. Input cards are specific to the software codes and are used to provide input data that are always needed. The data runs programs of scf, nscf, and bands to get the band structure and optimization of K points, Cutoff energy and Symmetry points. The PWscf modules supported by the software includes pw.x for the input data and pp.x for post processing.

The codes for data post processing (PP) in pp.x extract the specified data from files that were produced by pw.x, and prepares the data for plotting by writing them into formats that can be read by the plotting programs. These programs include bands.x, plotband.x and dos.x. The bands.x extracted files produced by pw.x that were necessary for band structure plotting. While plotband.x read the output of bands.x and produced band structures plots and the dos.x calculated electronic Density of States (DOS).

3.3 Structural and Electronic Properties of Tin Halide Perovskites

All density functional theory (DFT) calculations were performed using their respective Perdew-Burke-Ernzerhof (PBE) Norm conserving pseudopotentials. The PBE pseudopotentials of Tin, Hydrogen, Carbon, Nitrogen and Iodine ('Sn', 'H', 'C', 'N' and 'I') distributed within the QUANTUM ESPRESSO pseudo library were used for all calculations.

The cell shape and atomic positions were relaxed in DFT, using the standard PBE version of the GGA electron exchange-correlation functional.

The density of states function $g(E)$ is defined as the number of electronic states per unit volume, per unit energy for electron energies as stated by Mejia-Rodriguez *et al.,* (2021). The density of state function is important for calculations of effects based on

22

band theory in Fermi's Golden Rule, to find the rate of optical absorption. It also provides both the number of excitable electrons and the number of final states for an electron. In the calculations of electrical conductivity, it provides the number of mobile states, while in computing electron scattering rates it provides the number of final states after scattering.

The structural optimization was achieved by doing a variable cell relaxation as implemented in quantum espresso for self-consistent fields. A structural optimization of non-self-consistent fields for band structure calculation was also done where the atomic positions of the input file were not varied. Electronic structure calculation is done by using the desired K-mesh which gives the density of state calculation. The presence of the A, B and X different ions of the perovskite structure determines the photovoltaic performance, and hence the study of the electronic structure. The level of alignment to the electron and hole transporting media determines the maximum efficiency to be achieved for heterogeneous PIN junctions.

3.4 Optoelectronic Properties of Tin Halides

The important optoelectronic properties of semiconductors that may be computed include the light absorption and emission strength, ionization potentials, and their electron affinities, (Merdasa 2016). The hybrid functional GGA+U approximation was considered, and thus the optimization of convergence parameters with the aim of assessing how significantly the collective orientation of cations present influenced the position of the band gaps and hence the variation of the optical properties of tin halides.

3.5 Mechanical Properties of Tin Halides

The mechanical properties of DASnI3 was used to analyze the strain, the stress or fracture mechanics and even the deformation of solid absorber layers when this material is being used in photovoltaic. This was investigated by the stress-strain method based

on the first-principles calculations. The elastic constants were obtained by calculating the total energy by displacing ions from the ground state as a function of appropriate lattice deformation. The elastic strain energy was obtained by calculating full elastic constants which facilitate the complete mapping of Young's and shear moduli and Poisson's ratios along all crystallographic orientations with the aim of assessing the anisotropy in them.

3.6 Photovoltaic Application.

To determine the photovoltaic application of DASnI3 perovskite-based solar cell, the optical absorption characteristics is paramount. A good absorber material should have its absorption coefficiency high enough equivalent to the visible light for effective utilization of the solar radiation. The band gap of the absorber layer and the carrier characteristics relevant for entropic contribution due to the alignment between absorber and carrier transporting media were determined.

3.7 Derivation of the Governing Equations and Theorems

The simulation is based on the Density functional theorem, Born Oppenheimer approximations, Hohenberg and Kohn theorems and the Kohn sham equations which lead to the solution of the Schrödinger equation. The first step is the direct application of density functional theory (DFT) to the calculation of many body systems. The system provides a framework of understanding the collective behavior of a large number of interacting particles. DFT is the most powerful and widely used ab-initio method (Dreizler, R.M. and Gross E.K.U. 1990). It is based on the Hohenberg and Kohn (1964) theorem, which implies that all ground state properties of an inhomogeneous electron gas can be described by a functional of the electron density, and provides a one to one mapping between the ground-state density and the external potential. Kohn and Sham, (1965), states the fact that this one-to-one mapping holds both for an interacting and a

non-interacting system to define an effective non-interacting system, yields the same ground-state density as the interacting system.

3.7.1 The Many-Body System

To calculate the ground state energy of a collection of atoms the wave function below is used to describe the system,

$$H\Psi(\{r_i\},\{R\}) = E\Psi(\{r_i\},\{R_i\}).$$

… (3.1)

Here, H is the Hamiltonian operator and it is divided into two parts the kinetic energy operator T and the potential energy operator V.

$$\hat{H} = \hat{T} + \hat{V}_{coulombic}.$$

…(3.2)

In quantum mechanics we look at a single particle state hence Born Oppenheimer approximations are employed which states that the nuclei of atoms are big, heavy and slow in motion while the electrons are small light and move faster compared to the motion of the nuclei. This means that the time an electron needs to find the ground state with a specific position of the nuclei is much faster than the nuclei could move. Since the electrons move very fast, they only see the static positions of the nuclei. Hence the dynamics of the nuclei and electrons are decoupled.

$$\Psi(\{r_i\}R_i) = \Psi_N(\{R_i\}) * \Psi_e(\{r_i\})$$

… (3.3)

Thus, we concentrate on solving the ground state of electrons for a fixed set of atomic positions. The number of variables is then reduced thus the Hamiltonian now consists of electron terms only as shown below.

$$\hat{H}\psi(r_1,r_2,r_3...r_n) = \hat{E}\psi(r_1,r_2r_3...r_n)$$

… (3.4)

The Hamiltonian of the electron consists of three terms,

25

$$\hat{H} = -\frac{\hbar^2}{2m_e}\sum_{i}^{Ne}\nabla_i^2 + \sum_{i}^{Ne}V_{ext}(r_i) + \overset{Ne}{\Sigma}\Sigma U(r_i r_j) \qquad \dots (3.5)$$

The first term of the Hamiltonian consists of KE, the second term is the potential energy where the electrons are interacting with the nucleus that is seen as an external potential. The third term is the electron-electron repulsion. The particle is a many body 3N dimensional system. The approach of density functional theory which reduces the wave functions to electron density where 3N dimensions reduces to three spatial dimensions.

The electron density is given by;

$$n(r) = \psi^*(r_1, r_2, r_3, \dots, r_n)\psi(r_1, r_2, r_3, \dots r_n) \qquad \dots (3.6)$$

Considering an electron as a point charge in the field of other electrons this simplifies the many electron problem to many one electron problem below;

$$\psi(r_1, r_2 \dots r_n) = \psi_1(r_1) * \psi_2(r_2) * \psi_3(r_3) \qquad \dots (3.7)$$

We then define the single electron density in terms of all the single wave functions

$$n(r) = 2\sum_{i}\omega_i^*(r)\omega_i(r) \qquad \dots (3.8)$$

3.7.2 Hohenberg and Kohn Theorems

Basing on Hohenberg and Kohn theorems where the first theorem states that, the ground state energy of an electron is a functional of a function

$$F[f] = \int_{-1}^{1} f(x)dx \qquad \dots (3.9)$$

Therefore E is given as;

$$E = E[n(r)] \qquad \dots (3.10)$$

While the second theorem states that the ground state energy is obtained by minimizing the electron density thus;

$$E[n(r)] \rangle E_o[n_o(r)] \qquad \ldots (3.11).$$

The total energy is expressed in terms of the non-interacting auxiliary system as:

$$E_o = \min_\rho \sum [T_\rho] + \int V_{ext}(r)\rho(r)d^3r + \frac{1}{2}\int\int \frac{\rho(r)\rho r'}{|r-r'|}d^3r d^3r' + E_{xc}[\rho] \qquad \ldots (3.12)$$

Here the first term is kinetic energy of a non-interacting system with the density ρ, the second one is the potential energy of the external field $v_{ext}(r)$, connected to the coulombic interactions between electron and the nucleus the third term is the Hartree energy due to electron-electron repulsions, and the exchange-correlation energy $E_{xc}[\rho]$ entails all interactions, which are unknown and not included in the previous terms. They need to be approximated and take care of all the quantum mechanical interactions between electrons. The charge density $\rho(r)$ of the non-interacting system, which by construction equals the charge density of the full system, can be expressed through the orthogonal and normalized functions $\varphi_{i(r)}$ as;

$$\rho(r) = \sum_i^{occ} |\varphi_i(r)|^2 \qquad \ldots (3.13)$$

Variation of the total energy functional according to Slater (1937) with respect to the function $\phi_i(r)$ yields a set of equations, the Kohn-Sham (KS) equations, which have to be solved self-consistently, and which are of the form of a single-particle Schrödinger equation:

$$\left[-\frac{1}{2}\nabla^2 + v_n(r) + v_H(r) + v_{xc}(r)\right]\phi_i(r) = \varepsilon_i\phi_i(r) \qquad \ldots (3.14)$$

27

This scheme corresponds to a single-particle problem, in which electrons move in the effective potential,

$$v_{eff}(r) = v_n(r) + v_H(r) + v_{xc} + (r) \qquad \ldots (3.15)$$

The energy functionals stated by Slater (1937) provide in principle the exact ground state energy if the energy $Exc[\rho]$ due to the exchange-correlation is exactly known. This function is difficult to find, since this would be equivalent to the solution of the many-body problem. For applications, the exchange-correlation energy $Exc[\rho]$ is approximated basing on some known functionals. Some of the most popular approaches which are used include Perdew, Burke and Ernzerhof (PBE) and local-density approximation (LDA), in which the exchange-correlation energy $Exc[\rho]$ of an inhomogeneous system is approximated by the exchange-correlation energy of a homogeneous electron gas, standard density functional theory is designed for the study of ground state properties which can be evaluated accurately

The Kohn-Sham equation can be solved in some basis set. The wave function $\phi i(r)$ in the Kohn-Sham equation according to Szotek, (1954) can be represented as linear combination of N appropriate basis functions

3.7.3 The Kohn-Sham Equation
The Kohn Sham Equation is given by,

$$\varphi(r) = \sum_i^n c_i \phi_i(r) \qquad \ldots (3.16)$$

Where the basis set $\phi_i(r)$ corresponds to the specifics of the solving problem such as the crystal symmetry, the accuracy or special features of the electronic structures. According to the variational principle the differential equation (3.15) represented in the basis (3.16), can be transformed to a set of linear equations:

$$\sum_{i}^{N} \left(H_{ij} - \varepsilon S_{ij} \right) c_j = 0 \qquad j = 1,2,3...N \qquad \qquad \text{... (3.17)}$$

The matrices equations. 3.18 and 3.19 below are Hamiltonian and overlap matrices respectively

$$H_{ij} = \int d^3 r \phi_i^*(r) \hat{H}(r) \phi_i(r) \qquad \qquad \text{... (3.18)}$$

$$S_{ij} = \int d^3 r \phi_i^*(r) \phi_i(r) \qquad \qquad \text{... (3.19)}$$

Using the identity, the set of linear equations can be transformed to ordinary eigenvalue problem below;

$$\sum_{j}^{N} \left(\tilde{H}_{ij} - \varepsilon \delta_{ij} \right) \tilde{S}_j = 0 \qquad \qquad \text{... (3.20)}$$

This problem is solved by diagonalization of $\tilde{H}$.

3.8 The Exchange Correlation Functionals

Through the Kohn-Sham equation the ground state quantum mechanical many electron problem is reduced to self-consistent one electron form in DFT. Computing each part of DFT energy is easy, except the "exchange-correlation". This complicated exchange correlation energy functional can be obtained through the stated approximations.

3.9 Local Density Approximations (LDA)

Local density approximation has been one of the longest used standard choices in ab-initio DFT studies. It is simple and describes and interprets the atomic structure, elastic and also vibrational properties of semiconductor materials. The concept being the homogeneous electron gas is approximated as the exact exchange-correlation energies of an inhomogeneous system. They are important in studying the complexities of a system which brings about the high sensitivity to synthesis parameters necessitating first principles computations. The prediction of Fermi level and band structure are often

carried out using LDA incorporated in simulation packages such as in quantum espresso. This approach incorporates an exchange-correlation functional E_{xc}^{LDA} written in the form:

$$E_{xc}^{LDA} = \int n(r)\varepsilon_{xc}^{\text{hom}}(n(r))dr \qquad \ldots (3.21)$$

LDA has had realistic results in describing the atomic structure, elastic and vibrational properties of systems which are slow in density ratio and their chemical properties. However its shortcomings include lack of accuracy in describing the energetics of chemical reactions which tend to break down   and at times LDA puts crystals in qualitatively wrong energetic order. Thus this should be put in consideration in applications. LDA are important in the construction of other approximations such as Generalized Gradient Approximations or hybrid functionals.

3.10 Generalized Gradient Approximation (GGA)

This method is a continuation of LDA where it takes in account both the density of uniform electron gas and its deviation from homogeneity by considering the gradient of charge densities. This exchange-correlation energy is written in the form:

$$E_{xc}^{GGA} = \int \varepsilon_{xc} n(r)\nabla n(r)dr \qquad \ldots (3.22)$$

The GGA exchange correlation potential is written as:

$$V_{xc}(r) = \frac{dE_{xcG}}{dn(r)} = \frac{+dF_{xc}}{dn} - \sum_{\alpha=1}^{3} d\alpha\left(\frac{dF_{xc}}{d(d\alpha n)}\right)/n = n(r) \qquad \ldots (3.23)$$

Where $F_{xc}\left(n,|\nabla n|\right) = E_{xc}\left(n, \nabla\right)n$, and $\partial\alpha$ stands for gradient component GGA improved significantly the LDA's description of the binding energies for real systems. However, LDA and GGA both have a limitation when describing the correct electronic properties of some materials for instance the transition metal oxides and the strongly correlated systems.

3.11 GGA+U Hybrid Functional Approximations

Semiconductors are some of the vital technological materials with numerous applications especially in solar cells. First principles approaches that illustrate their properties accurately are very important. From earlier studies it has been established that the band gaps obtained by both LDA and GGA are underestimated for semiconductors, while the application of Hartree-Fock method overestimates their band gaps. Therefore necessitates the use of hybrid functionals GGA+U developed from GGA.

Basing on its formulation, GGA functional effectively contains a screened mean-field representation of many-body behavior while DFT+U formalism represents the correlated physics of a many-body impurity system in a single particle framework. To make these correlations explicit in DFT+U, the GGA energy is supplemented with a local moment term similar to that appearing in Hubbard model as stated by Folk *et al.,* (1957) and Novoselov *et al.,* (2005) In the Hamiltonian given as $E_{Hub}\left[\left\{n_{mm}^{I\sigma}\right\}\right]$ the double counted GGA correlation $E_{Dc}\left[\left\{n^{I\sigma}\right\}\right]$ is subtracted to get;

$$E_{GGA}+_{U}\left[n(\vec{r})\right] = E_{GGA}\left[n(\vec{r})\right] + E_{Hub}\left(n_{mm'}^{I\sigma}\right) - E_{DC}\left[\left\{n^{I\sigma}\right\}\right] \qquad \ldots 3.24$$

From equation 3.24 $n(\vec{r})$ is the spatial electron density while $n_{mm'}^{I\sigma}$ denotes the atom-centered spin-orbital occupation of the Ith atom. This is where the Hubbard correction is placed indexed by spin σ and angular momentum projection m. The term $E_{DC}[\{n^{I\sigma}\}]$ depends solely on the net spin-resolved orbital occupation $n^{I\sigma} = \sum_m n_{mm}^{I\sigma}$. To conveniently represent $n_{mm'}^{I\sigma}$ the valence electronic wave function Ψ_k^{σ} is projected with wave vector $\bar{k}$ and spin σ onto atom-centered spin orbital states Φ_m^I so that

$n_{mm'}^{I\sigma} = \sum_k f_k \langle \psi_k^{\sigma} | \phi_{m'}^I \rangle \langle \phi_m^I | \psi_k^{\sigma} \rangle$ where f_k is the weight of the kth state.

The calculations presented are performed in a formalism invariant under rotation of the atomic orbital basis set according to Lichtenstein *et al.,* (2001) and Liechtenstein *et al.,* 1995 thus defining the localized occupancies. This means, $E_{Hub}\left[\left\{n_{mm'}^{I\sigma}\right\}\right]$ is determined by the screened Coulomb interaction U and exchange interaction J parameters .In this case, the Hubbard correction to the Kohn–Sham functional assumes the form

$$E_U n_{mm'}^{I\sigma} = \frac{U}{2} \sum_I \sum_{m\sigma} n_{mm}^{I\sigma} - \sum_{m'} n_{mm'}^{I\sigma} n_{m'm}^{I\sigma} \qquad \dots 3.25$$

$$= \frac{U}{2} \sum_{I\sigma} Tr\left[\hat{n}^{I\sigma}\left(1 - \hat{n}^{I\sigma}\right)\right] \qquad \dots 3.26$$

This introduces a set of localized orbitals that diagonalize the occupation matrices $\hat{n}^{I\sigma}$ simplifying the correction E_U to;

$$E_U n_{mm'}^{I\sigma} = \frac{U}{2} \sum_{I\sigma} \sum_i \lambda_i^{I\sigma} 1 - \lambda_i^{\sigma} \qquad \dots 3.27$$

It can be seen that for a fully unoccupied $\left(\lambda_i^{I\sigma} = 0\right)$ or a fully occupied $\left(\lambda_i^{I\sigma} = 1\right)$ the term is vanishing. The value U admits a physical interpretation of additional energetic cost assuming partial orbital occupancy given as $\lambda_i^{I\sigma} \in (0,1)$. This term corrects over the counting of the Coulomb self–interaction energy for partially occupied DFT orbitals common within the LDA and GGA approximations, thus mimicking an open quantum system.

Hubbard U is viewed as a correction to LDA and GGA, setting U to be equal to the curvature of the energy functional obtained through a linear response method according to 42, the single-particle potential V^{GGA} is perturbed to yield $V' = V^{GGA} + \sum_I \alpha_I P^I$. Here α_I is the strength of the localized potential and P^I is a d-level projector for the Ith corrected atom. The problem is then reduced to the minimization of total energy

$$E[\{q_I\}] = \min{}_{n(r),\alpha I} E[n(r)] + \sum_I \alpha_I (n_I - q_I) \qquad \dots 3.28$$

Where α_I takes the role of a Lagrange multiplier employed to enforce the orbital occupancy restraint. The Hubbard U term is then defined as;

$$u = \frac{\partial^2 E[\{q_I\}]}{\partial q_I^2} - \frac{\partial^2 E^{GGA}[\{q_I\}]}{\partial q_I^2} \qquad \dots 3.29$$

For practical implementation, a Legendre transformation is performed that shifts dependence to the α_I parameter reducing the sum in equation 3.29 to $\sum_I \alpha_I n_I$ term. The Hubbard U may then be written in terms of generalized susceptibilities as

$$\chi_{IJ} = \frac{\partial n_I}{\partial \alpha_J} \quad \text{and} \quad \chi_{IJ}^0 = \partial n_I / \partial \alpha_J^{GGA}$$

$\chi_{IJ} = \partial n_I/\partial \alpha_J$ that yields

$$U = \left(\left(\chi_{IJ}^{0} \right)^{-1} + \chi_{IJ}^{-1} \right)$$

… 3.30

The bare susceptibility χ_{IJ}^{0} is accordingly derived by performing the DFT calculation at $\alpha_I = 0$ with fixed U_{in}, and the orbital occupancy response χ_{IJ}^{0} obtained through successive calculations at varying values of α_I using initial orbital occupancies from the bare calculation. The derived U then corresponds to a potential arising from redistribution of occupancies throughout the system subsequent to an induced perturbation on a d level and accompanying the electronic correlation at the perturbed site. The self-consistent value U_{SCF} then corresponds to the electron–electron interaction present in the GGA functional component of the GGA+U state when $U = U_{in}$.

3.12 Self-consistent Iterative Solution

Density Functional Theory is a method used to describe a system with the use of electron density. DFT is used in predicting and analyzing the electronic and optical properties of materials where the electronic density distribution n(r) is considered. Presently, DFT is applied in many first principles or the ab-initio codes. The sequence scheme for calculation of materials property can be generalized as shown in the figure 3 below.

Figure 3

Schematic Flow of the Solution of the Schrödinger Equation to Obtain Self-Consistent Electronic Density
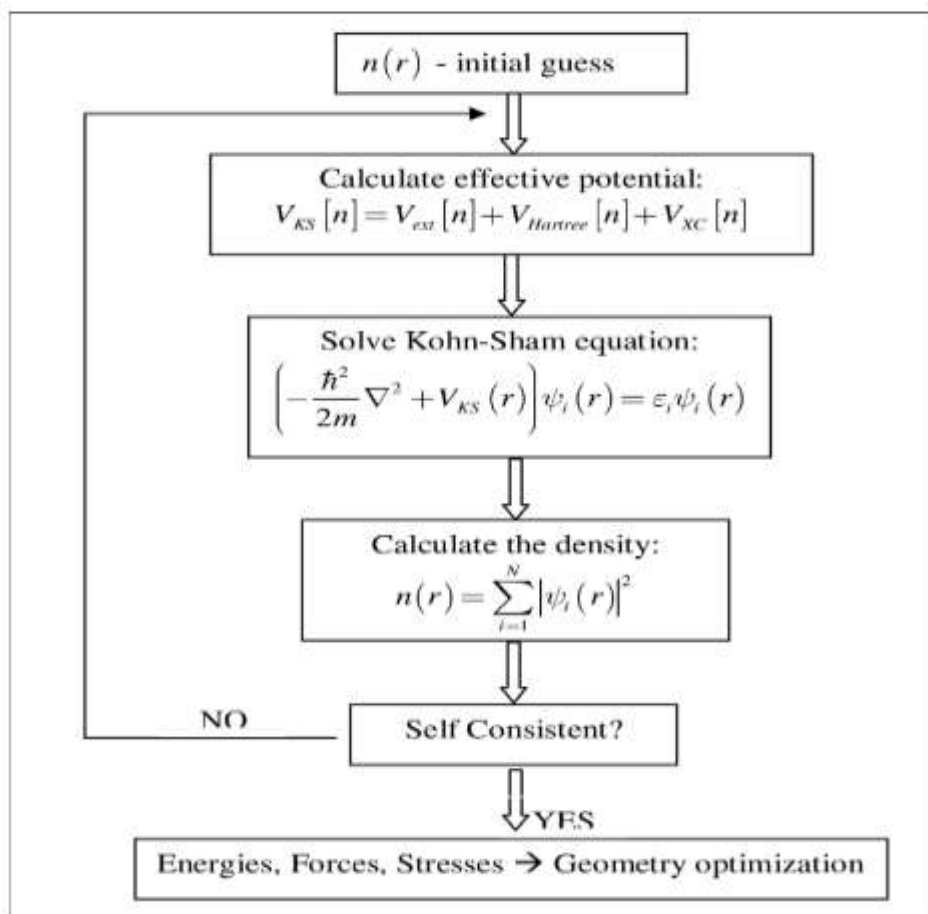
Adapted from Ciucivara, (2007).

The first step is to choose or construct the fixed nuclear ionic positions. While the second step determines the initial condition of a system, that is the distribution of the charge density where there is the superposition of charge densities.

The choice of basis set involves the choosing of the initial data which significantly is different from the solution or the optimization of the parameters. This stage determines

the choice of the advanced estimation of the crystal grid and as well as the atomic orbitals. The next step is to solve the Schrödinger equation. This is done by determining the density of single electron wave functions since it is impossible to solve the equation with more than one electron system in an atom, Iljasov *et al*., 2014. In this way some properties of electrons are not considered but at the same time it becomes possible to solve the Schrödinger equation in some variants Nelasov *et al.,* 2011. Thus, the results can be used to determine different material parameters for example, in calculating the geometrical parameters of a crystal grid and also the energy connection between its points Kravcova *et al.*, (2011) and Kazakova, (2009). The results obtained for the atomic structures from parameter calculations can be used to determine the strength of the material according to Iskandarov *et al*., (2012). Kravcova *et al.*, (2011) and Babkin *et al.*, (2011) argue that the parameter calculation results can also be used to determine the electron structure properties, the band structure, the magnetic characteristics and many more other properties such as formation of grain boundaries and the optical properties.

3.13 Implementation
3.13. Plane Waves

The Density Functional Theory (DFT) and the Born-Oppenheimer approximation were used as a link between the interactions of the nuclei and the electrons commonly known as many body problem that leads to the single particle problem moving in an effective potential for a set of 60 stationary nuclei. In this approach, a single particle eigenstates is expanded into a basis set of plane waves. The plane waves are used due to the fact that the eigenstates are exact for the electron gas which is homogeneous and not specified to any particular atom. The expansion of the plane-waves in the Kohn-Sham wave function is important when calculating the total energy of solids which is periodic.

The solution of this single-particle Schrödinger equation within a periodic potential, is itself periodic and thus obeys the Bloch's theorem below;

$$\varphi kj(r) = \mu kj(r)e(ikr) \qquad \ldots (3.31)$$

In the equation, k is the crystal momentum and j is the band index that classifies the electronic states that have the same k-vector defined within the first Brillouin Zone. The periodicity of the crystal is $\mu_{kj}(\mathbf{r})$ which is solved using a basis set;

$$\varphi kj(r) = \sum_G cjG = kei(K+G)r \qquad \ldots (3.32)$$

G can be defined by the equation b= 2πm, where b are the lattice vectors of the crystal while m is an integer. Expanding the equation leads to;

$$\varphi_{kj} = \sum_G cj, k + Ge^{ik} r\mu_{kj}(r) \qquad \ldots (3.33)$$

When the Bloch states are used, the Kohn-Sham equation will be;

$$\left[\frac{-h}{2m}\nabla^2 + Veff(r) \right]\mu kj(r) = \sum kj\mu kj(r) \qquad \ldots (3.34)$$

Veff can be defined as V eff (r) defined as:

$$V_{eff}(r) = V_{ext}(r) + V_H(r) + V_{xc}(r) \qquad \ldots (3.35)$$

Where V ext, is the external potential due to the interaction with the nuclei, V H is the Hartree associated with electrons interaction and V xc is the exchange correlation potential.

The Fermi energy is obtained from the equation below;

$$n(r) = \frac{2\Omega}{2\Pi 3} \sum_j \int |\mu kj(r)|2\Theta\left(Ef - \sum_{kj}\right) d3k \qquad \text{… (3.36)}$$

The factor 2 takes care of spins up and down i.e. ↑ and ↓ and the Θ in the equation is a step function which can be 1 or 0. Fermi energy E_F is the highest energy level occupied by a single particle and is defined by the number of electrons in the unit cell. This energy is termed as Fermi energy given by;

$$\int n(r) d^3 r = N \qquad \text{… (3.37)}$$

The electronic wave functions are expanded into k-points described in a form of discrete set of plane waves according to Bloch's theorem which merges the number of electronic states of infinite problems to a finite number of electronic states at an infinite number of k-points extended over a single unit cell. This could be a minor improvement since an infinite number of calculations for the different k-points is needed. Since the electronic states at k- points which are close to each other are similar, there is a possibility of representing the wave functions of a specific point by the wave function at a single k-point for a k-space.

3.14 The Brillouin Zone (Reciprocal Space) and K-Points

Density Functional Theory is used in materials research for calculations in a system of periodic atoms in space. A supercell is a cell with atoms repeated periodically; these supercells are identified with the lattice vectors a 1, a 2 and a 3. The solutions of the Schrödinger equations for a periodic system, must be in line with Bloch's theorem written as:

$$\varphi_k(r) = e(ikr)\mu k(r) \qquad \text{… (3.38)}$$

Where k is a wave vector which is associated with the First Brillouin zone while r, represents the position vector which defines a point in space

$$\mu_k(r) = \mu_k\left(r + n_1\alpha_1 + n_2\alpha_2 + n_3\alpha_3\right)$$ … (3.39)

From the equation, the integers n_1, n_2, n_3 are periodic functions and the space is periodic for a super cell with the same periodicity. The Schrödinger equation can be solved independently for any value of k as indicated by Bloch's theorem. Sholl & David, 2009, states that the mathematical problems are simpler to solve with respect to k than r, involved in DFT. (Because the expansion of e ik(r) expresses the original plane waves and calculations related in this equation are defined as plane-wave calculations. Plane waves take advantage of the first Fourier transformation (FFT), hence it is a numerically convenient basis set which can be used in DFT. The real space is represented by the vector r while the reciprocal space is represented by the vector k (or k space). In k space, a unit cell has a minimum volume that contains all the information of the material. The primitive cell concept in k space follows the Wigner-Seitz cell, where the reciprocal lattice vectors are easily defined like in real space. Cells in k space are referred to as the Brillouin zone, the Brillouin Zone contains several k-points with special significance of symmetry. These points are given independent identities. one of the most important being the Gamma point (Γ point), which is the center of the reciprocal space which implies; k= 0 at the Γ point, (Sholl & David, 2009).The convergence of k-point mesh ($n_i \times n_j \times n_k$), where n_i =1, 2, 3 with respect to total energies for the orthorhombic structure of the DASnI3 is shown in the Figure 4 below;

Figure 4

Graph of Energy Versus K-Points
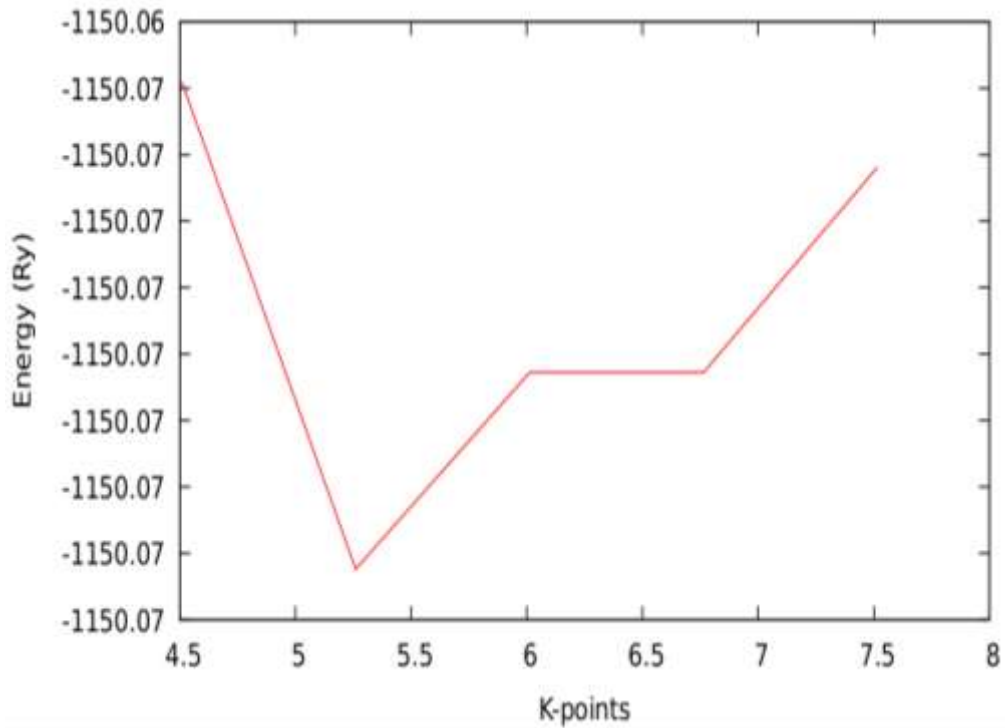
The Plane wave basis energy is calculated based on DFT in the study of a material. The cut-off energy optimization is examined at a constant k-point-mesh obtain prior. The experimental lattice parameters are achieved from the crystallographic databases. The curve below is the cut-off optimized energy for the DASnI3 structure

Figure 5

Cut-Off Energy Curve for DASnI3
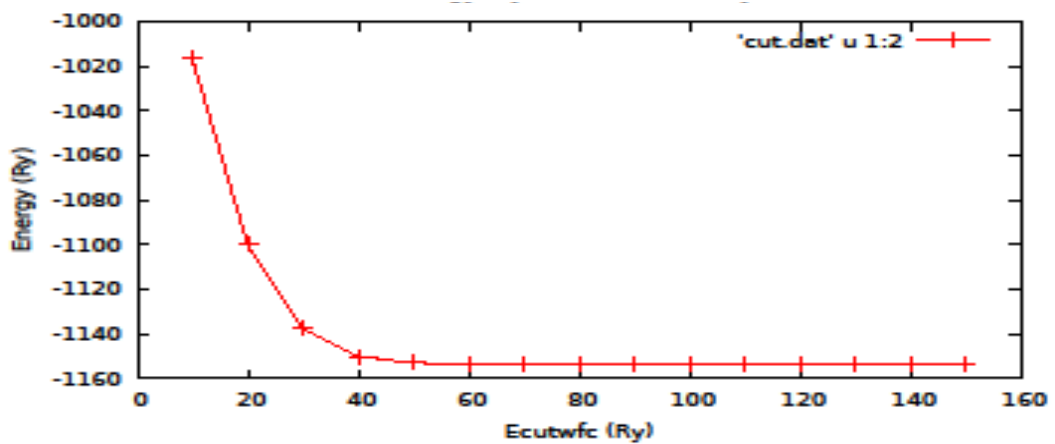
The convergence test of the plane-wave energy cut-off and also the k-point grid was determined at fixed lattice constants and the atomic position relaxed at a temperature of 0K. Volume was varied while relaxing the atomic coordinates a significant principle for every DFT calculation. The convergence of the energy cut-off in relation to the total energy was determined by choosing a k-point grid for which the results are expected to converge then the system simulatedin QE by gradually increasing values of Energy Cut off .The values obtained for the Energy Cut off ECUT and their output Energy values in Rydberg was plotted as shown in Figure 5 above .From the figure it indicates that energy cut-off less than 50 Ry is inadequate therefore, values greater than 50 Ry should be selected. However greaterenergy cut-off does not increase precision but it raises CPU time thus increasing the computation cost but does not temper with accuracy.

3.15 Elastic Constants

The elastic constants for DASnI3, was performed by an accurate structural relaxation of the material, to approximately zero stress state of the structure. Subsequently application of perturbations to the lattice vectors follows and the resulting stress tensor is calculated allowing relaxation of the ionic degrees of freedom. The constitutive relations from linear elasticity which relate stress and strain are finally employed that fits the full 6x6 elastic tensor .The face centered orthorhombic phase has three lattice parameters a , b and c. Bravais lattice vector of the orthorhombic phase according to Nyawere *et al.,* (2014), has a matrix of the form;

Table 2

Elastic Constant Matrix.

$$
\begin{bmatrix}
c_{11} & c_{12} & c_{13} & c_{14} & c_{15} & c_{16} \\
c_{12} & c_{22} & c_{23} & c_{24} & c_{25} & c_{26} \\
c_{13} & c_{32} & c_{33} & c_{34} & c_{35} & c_{36} \\
c_{14} & c_{42} & c_{43} & c_{44} & c_{45} & c_{46} \\
c_{15} & c_{52} & c_{53} & c_{54} & c_{55} & c_{56} \\
c_{16} & c_{62} & c_{63} & c_{64} & c_{65} & c_{66}
\end{bmatrix}
$$

From the matrix, the nine elastic constants for the orthorhombic phase are; C_{11}, C_{22}, C_{33}, C_{44}, C_{55}, C_{66}, C_{12}, C_{13} and C_{23} which are the corresponding strain energy that can be obtained. From the elastic tensor defined above, a number of aggregate and derived properties are calculated. The properties include Voigt and Reuss bounds on the bulk and shear moduli. For instance, the elastic constants are generated from energy variation by applying a little strain to the converged lattice configuration. This energy can be written as:

$$\nabla E = \frac{v}{2} \sum_{i=1}^{6} \sum_{j=1}^{6} c_{ij} e_i e_j \qquad \ldots (3.40)$$

From the equation, *V* is the volume of the original lattice cell while ΔE is the energy increase from the strain with the vector $e = e_1 e_2 e_3 e_4 e_5 e_6 e_7 e_8 e_9$ *C* is the matrix of the elastic constant. For the orthorhombic phase dimethyl ammonium tin triiodostanate II in which the primitive vectors can be denoted as;

$$R = \frac{1}{2}b\left(0,1,\frac{c}{b},\frac{a}{b},0,\frac{c}{b},\frac{a}{b},1,0\right) \qquad \ldots (3.41)$$

R can be strained according to the relation in the deformed matrix with distorted lattice vectors

Strain on c_{11} defined by uniaxial deformation along (0, 0, 1) to obtain;

$$\frac{\nabla E}{v} = \tau_1 \delta + \frac{c_{11}}{2}\delta^2 \qquad \ldots (3.42)$$

c_{22} Was obtained by applying the strain on (0, 1, 0) to obtain;

$$\frac{\Delta E}{v} = \tau_2 \delta + \frac{c_{22}}{2}\delta^2 \qquad \ldots (3.43)$$

c_{33} Was obtained through deformation along (0, 0, 1)

$$\frac{\Delta E}{v} = \tau_3 \delta + \frac{c_{33}}{2}\delta^2 \qquad \ldots (3.44)$$

c_{44} Obtained through (1, 0, 0)

$$\frac{\Delta E}{V} = 2\left(\tau_5 \delta + c_{55}\delta^2\right) \qquad \ldots (3.45)$$

c_{55} Was through

$$\frac{\Delta E}{V} = 2\left(\tau_5 \delta + c_{55}\delta^2\right) \qquad \ldots (3.46)$$

c_{66} Along (0, 0, 1)

$$\frac{\Delta E}{v} = 2\left(\tau_6 \delta + c_{66}\delta^2\right) \qquad \textbf{...} (3.47)$$

c_{12} Through (1, 1, and 0) to obtain;

$$\frac{\Delta E}{v}(\tau_1 - \tau_2)\delta + \frac{1}{2}\left(c_{11} + c_{22} - 2c_{12}\delta^2\right) \qquad \dots (3.48)$$

c_{13}

$$\frac{\Delta E}{v}(\tau_1 - \tau_3)\delta + \frac{1}{2}\left(c_{11} + c_{33} - 2c_{23}\delta^2\right) \qquad \dots (3.49)$$

c_{23}

$$\frac{\Delta E}{v} = (\tau_2 - \tau_3)\delta + \frac{1}{2}\left(c_{22} + c_{33} - 2c_{23}\delta^2\right) \qquad \dots (3.50)$$

The Bulk modulus for the orthorhombic phase derived from elastic constants was given as;

$$\frac{\Lambda}{\left(1 + \gamma + \sigma\right)^2} \qquad \dots (3.51)$$

Where $\Lambda = c_{11} + 2c_{12}\gamma + c_{22}\gamma^2 + 2c_{13}\sigma + c_{33}\gamma\sigma$ \qquad ... (3.52)

$$\sigma = \frac{(c_{11} - c_{22})(c_{33} - c_{13}) - (c_{23} - c_{13})(c_{11} - c_{13})}{(c_{33} - c_{13})(c_{22} - c_{12}) - (c_{13} - c_{23})(c_{12} - c_{23})} \qquad \dots (3.53)$$

$$\gamma = \frac{(c_{11} - c_{22})(c_{33} - c_{13}) - (c_{23} - c_{13})(c_{11} - c_{13})}{(c_{22} - c_{12})(c_{33} - c_{13}) - (c_{12} - c_{23})(c_{13} - c_{23})} \qquad \dots (3.54)$$

The isotropy in elastic constants are obtained from appropriate averaging procedures which include the bulk, shear and Young modulus. The three commonly used averaging methods which are implemented in Thermo_pw code are the Voigt approach (Voigt, 1928), where in this approach a uniform strain is assumed, and the Reuss procedure

validates the uniform stress (Reuss, 1929). Combination of the Voigt and Reuss moduli results in a stiffness constant.

Bulk and shear modulus Voigt average for polycrystalline material is given as;

$$B_v$$

$$9kv = (c_{11} + c_{22} + c_{33}) + 2(c_{12} + c_{23} + c_{31}) \qquad \dots (3.56)$$

$$G_v$$

$$15G_v = (c_{11} + c_{22} + c_{33}) - (c_{12} + c_{23} + c_{31}) + 3(c_{44} + c_{55} + c_{66}) \qquad \dots (3.57)$$

While the Reuss Bulk and shear modulus are given by;

$$B_R$$

$$\frac{1}{k_R} = (s_{11} + s_{22} + s_{33}) + 2(s_{12} + s_{23} + s_{31}) \qquad \dots (3.58)$$

$$G_R$$

$$\frac{15}{GR} = 4(s_{11} + s_{22} + s_{33}) - 4(s_{12} + s_{23} + c_{31}) + 3(s_{44} + s_{55} + s_{66}) \qquad \dots (3.59)$$

According to the Voigt-Reuss-Hill (VRH) approximation (Hill, 1952) the shear and bulk moduli of the polycrystalline material were approximated as the mean of the Voigt and Reuss limit

$$B_{VRH}$$

$$2K_{VRH} = (K_v + K_R) \dots \qquad \dots (3.60)$$

G_{VRH}

$$2G_{VRH} = \left(G_V + G_R\right) \qquad \qquad \text{… (3.61)}$$

From bulk modulus and shear modulus, the Young modulus was obtained as;

$$A^\upsilon = 5\left(\frac{G_V}{G_R}\right) + \left(\frac{K_V}{K_R}\right) - 6 \geq 0 \qquad \qquad \text{… (3.62)}$$

While the Poisson's ratio was obtained from;

$$\mu = \frac{(3k_{VRH} - 2G_{VRH})}{(6k_{VRH} + 2G_{VRH})} \qquad \qquad \text{… (3.63)}$$

3.16 Optical Properties

Optical properties are the study of the interaction of light waves with the material medium. The properties can be obtained through the study of polarization and the absorption of electromagnetic radiation within the medium. These are expressed in terms of the dielectric constant ε_1, the conductivity σ_1, and the permeability μ_1 present in matter. To understand the properties well, it requires the definition of the complex refractive index as a new response function which is written in the form;

$$\hat{N} = n + ik = \left[\varepsilon_1 \mu_1 + i\frac{4\pi\varepsilon_1\sigma_1}{\omega}\right]^{\frac{1}{2}} = \left[\hat{\varepsilon}\mu_1\right]^{\frac{1}{2}} \qquad \qquad \text{… (3.64)}$$

The refractive index of the material (*n*), is written in terms of conductivity (σ_1), the permeability (μ_1), and the dielectric constant (ε_1) and also using the same constants, the extinction coefficient (*k*) can be written as eqn. (3.58) below (Gajdoš *et al.,* 2006)

$$\hat{n}^2 = \frac{\mu_1}{2}\left\{\varepsilon_1^2 + \left(\frac{4\pi\sigma_1}{\omega}\right)^2\right\}^{\frac{1}{2}} + \varepsilon_1 \qquad \qquad \text{… (3.65)}$$

$$\hat{k} = \frac{\mu_1}{2} \left\{ \left[\varepsilon_1^2 + \left(\frac{4\pi\sigma_1}{\omega} \right)^2 \right] \right\}^{\frac{1}{2}} \qquad \text{... (3.66)}$$

The two Equations above (3.65) and (3.66) are vital electromagnetic wave propagation relations in materials. To study the current properties of materials, polarization and absorption of electromagnetic radiation within the material medium is expressed in terms of dielectric functions. The dielectric functions are represented mathematically by the relation below

$$\varepsilon(\omega) = \varepsilon_1(\omega) + \varepsilon_2(\omega) \qquad \text{... (3.67)}$$

The reflectivity of the dielectric material without losses i.e. $K \to 0$ can be written in terms of refractive and extinction coefficient k and becomes:

$$\hat{q} = \frac{\omega}{c} \hat{N} = \frac{n\omega}{c} + i \frac{k\omega}{c} \qquad \text{... (3.68)}$$

$$n^2 - k^2 = \varepsilon_1 \mu_1 \qquad \text{... (3.69)}$$

$$2nk = \frac{4\pi\mu_1\sigma_1}{\omega} \qquad \text{.... (3.70)}$$

Writing equation (3.70) in terms of dielectric constant, permeability and conductivity gives,

$$\hat{N} = \mu_1 \left[\varepsilon_1 + i \frac{4\pi\sigma_1}{\omega} \right] = \mu_1 \hat{\varepsilon} \approx \frac{4\pi i \mu_1 \sigma_1}{\omega} \qquad \text{... (3.71)}$$

Noting that when $|\varepsilon_1| \geq 1$ then,

$$|\hat{N}| = \left(n^2 + k^2 \right)^{\frac{1}{2}} \qquad \text{... (3.72)}$$

3.17 Reflectivity

The reflectivity $R(\omega)$ can also be expressed mathematically as,

$$R(\omega) = \left[\frac{1 - \hat{N}}{1 + \hat{N}}\right]^2 = \frac{(1-n)^2 + k^2}{(1+n)^2 + k^2} \qquad \dots (3.73)$$

If K tends to 0, then reflectivity reduces to;

$$R = \left|\frac{1-n}{1+n}\right|^2 \qquad \dots (3.74)$$

The imaginary dielectric function $\varepsilon_1(\omega)$ was obtained by summing over conduction bands as stated by Ambrosch & Sofo (2006).

$$\varepsilon^1_{\alpha\beta}(\omega) = \frac{4\pi^2 e^2}{\Omega} \frac{1}{q^2} \lim_{q \to 0} \sum 2w_k \delta(\in_{ck} - \in_{vk} - \omega) \times \langle u_{ck+eqq} \mid u_{vk} \langle u_{ck+eqq} \mid u_{vk} \rangle \qquad \dots (3.75)$$

Equation (3.75) above is an indication of a transition between the occupied and the unoccupied states within the first Brillouin zone where the k vector waves are fixed. According to (Harrison, 1999) the Kramers-Kronig relation connects the real and the imaginary parts of an analytical dielectric function by;

$$\varepsilon^1_{\alpha\beta} = 1 + \frac{2}{\Pi} p \int_0^\infty \frac{\varepsilon^2_{\alpha\beta}(\omega')\omega'}{\omega^2 - \omega^2 + i\eta} d\omega' \qquad \dots (3.76)$$

 The complex dielectric constant $\hat{\varepsilon}$ and the conductivity $\hat{\sigma}$ are the prime response functions to the applied electric field.

3.18 Absorption Coefficient

The absorption coefficient $I(X) = I_o \exp(-ax)$ corresponds to the intensity loss per unit length and is given as:

$$\alpha(\omega) = \frac{\omega}{4\pi} \varepsilon_2(\omega) \qquad \dots (3.77)$$

The equation indicates that there is a strong relationship between $\alpha(\omega)$ and $\varepsilon_2(\omega)$.

The frequency dependent dielectric matrix was calculated using quantum espresso hybrid functionals where the imaginary and the real dielectric values of DASnI3 were obtained.

CHAPTER FOUR

DATA ANALYSIS PRESENTATION AND DISCUSSION

4.1. Introduction

This chapter discusses the results, data on the structural properties, the electronic, the elastic, the dielectric constants and the photovoltaic application of tin halide perovskites and also compares the results obtained from this work and other researches of perovskite materials from first principle and other works.

4.2 Structural Properties of DASnI3

An orthorhombic phase of DASnI3 with 60 atoms per cell space group Pna2$_1$ was considered. The original structure from the database and the optimized structure were simulated using the same values for ecutwfc and ecutrho and using XCrySDen according to Kokalj (1999) the structures were visualized before and after optimization. Figure 5 shows the structure of Dimethylammonium triidostanate II which decomposes to $H_4C + H_4IN + SnI_2 + C$. The lattice parameters obtained was $a = 8.505$ Å, $b = 9.232$ Å and $c = 15.04$ Å. Murnaghan's equation of state was used according to Madsen *et al.,* (2016) for volume optimization by minimizing the total energy with respect to the volume. The relationship between the energy and volume of the orthorhombic perovskite cell is represented by the energy-volume diagram (Fig.6); the PBE-XC functional results in a minimum energy at the volume 1151.507 Å^3

The C$_2$H$_8$N$_1$Sn$_1$I$_3$ structure was created by use of xcrysden software in the QE code to achieve optimized structure as shown in figure 6 below.

Figure 6

The Structure DASnI3 Perovskite Containing a Network of $H_4C + H_4IN + SnI_2 + C$
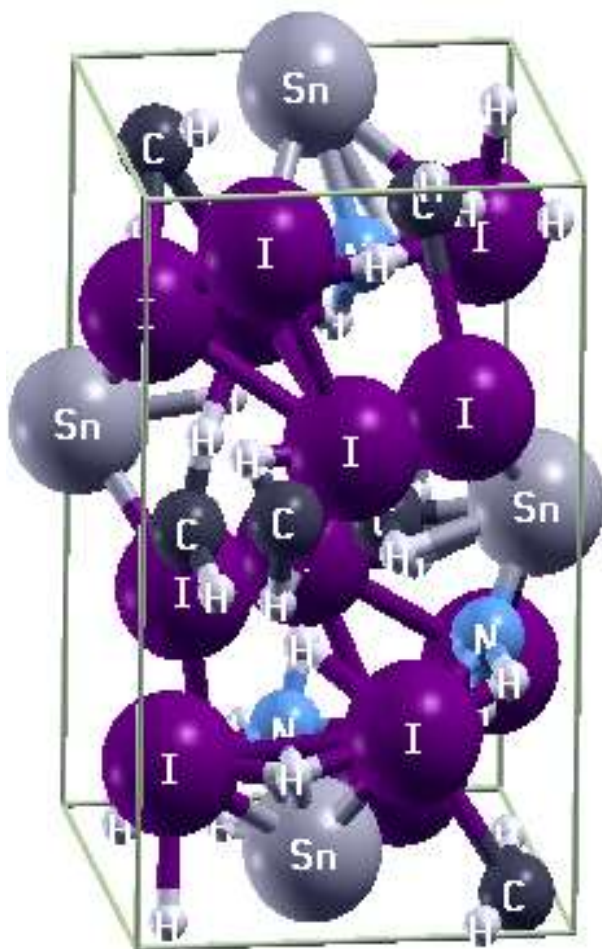
4.2.1: Lattice Parameters

The structural properties in terms of lattice constant for the DASnI3 was obtained as

8.5 angstrong . the results showed that dimethylammonum triidostanate II (DASnI3)

was stable and relaxed at 1151.5Ry as shown in figure 7 below.

Figure 7

Graph of Total Energy per Cell Minimum of 1151.5Ry Against Volume of Lattice Constants at 8.5Å
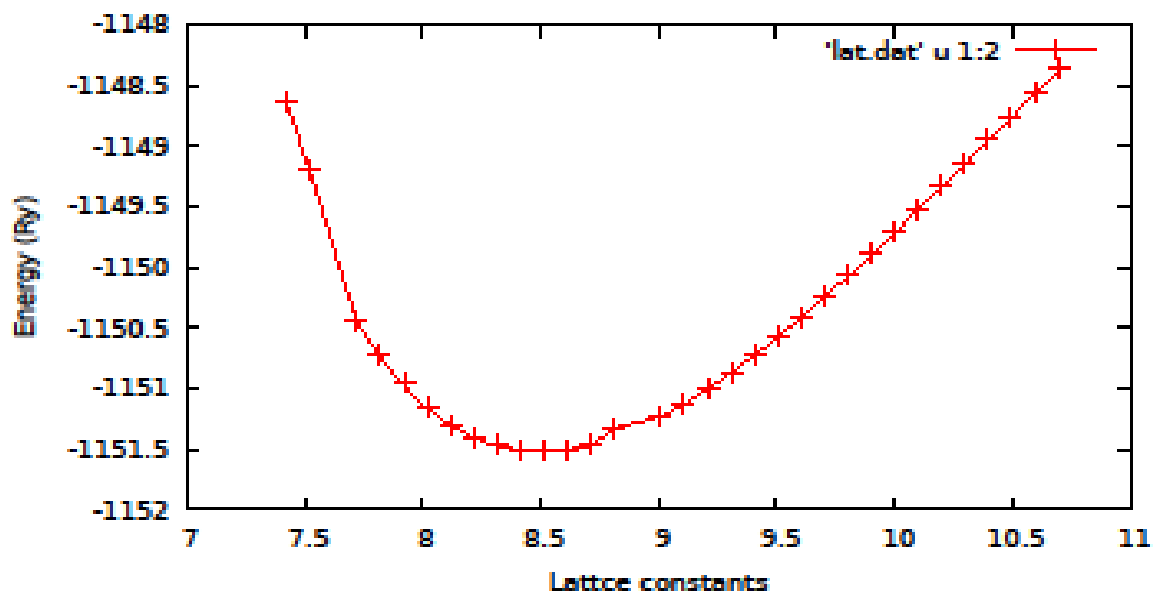
The electronic structures are determined by studying the band gaps and volume for Dimethyl Ammonium triiodostannate (II). The table below presents the values obtained from Lattice constants, volume per atom and band gaps from this research and those obtained from other related research. It is observed that Dimethyl Ammonium (DA) being larger in size than methylammonium (MA), results in to an increased band gap modifying the lattice constant (Hautzinger *et al*., 2020). The bonding between the metal and halide has a direct impact on the valence band and the conduction band positions. The extent of the orbital overlap is influenced by the A-site cation. Philippe, *et al* (2017) states that this change of composition, for instance, when DA is used as the A site cation the band gap of the perovskite increases as compared with MA perovskite.

Table 3

Value of Lattice Constants, Volume Per Atom and Calculated Band Gaps of DASnI3 in Comparison with other Studies.

	a($\dot{A}$)	b ($\dot{A}$)	c($\dot{A}$)	V 0 ($\dot{A}^3$)	Band gap values(eV)	References
QE PBE	8.505	9.232	15.040	1151.5	2.7	present work
VASP PAW	8.562	9.165	15.031	274.5032	2.834	Jain *et al* (2011)
QE LDA PZ Expt(DA 3 BiI 6)	30.8173	30.8173	8.8171	-	2.98 2.14	Zhao *et al* 2021
FPLAPW + lo WIEN2k EASnI 3	6.517	-	-	276.78	1.30	Joshi *et al* (2020)
FPLAPW Wein2k package Cs 2 InBiI6	12.32	-	-	1561.07	1.37	said *et al* (2021)
C2H8l3NSn SnI3 Expt	14.637	8.786	8.288	1065.8	-	Hecken, G(1993)

From the results presented in table 3 above, a correlation exists between the calculated band gap value of 2.7 and those obtained by Jain *et al.,* (2011) with a band gap of 2.8 eV for the same material. The lattice constants values are also closely related. It is also evident that the results are comparable from the smallest deviations seen and also compares well with other calculated values.

4.3 Electronic Properties

4.3.1 Electronic Properties of DASnI3

The electronic properties of the hybrid halide perovskites are of much importance and need to be studied because these materials are potential light-harvesting mediums. We employed PBE-GGA ex-change correlation potentials to study various electronic properties such as electron density plot, the band structure and energy band gap, the Density of states (DOS), and the partial density of states (PDOS) calculation. The band structure and the density of states (DOS) are important in analyzing the electronic properties of material.

The calculated band structure of the orthorhombic phase DASnI3 ($C_2H_8N_1Sn_1I_3$) crystal along the high-symmetry lines in the first Brillouin zone is presented in figure 8 below. The orthorhombic crystal has a direct bandgap at gamma symmetry points with 2.7eV calculated band gap energy from PBE, DFT exchange–correlation functionals. The Fermi level is located between the valence band maxima and the conduction band minima of the material. The diagram below shows the band structure of the dimethylammonium tin triiodide.

Figure 8

Graph of Calculated Band Gap against High Symmetry Points of DASnI$_3$
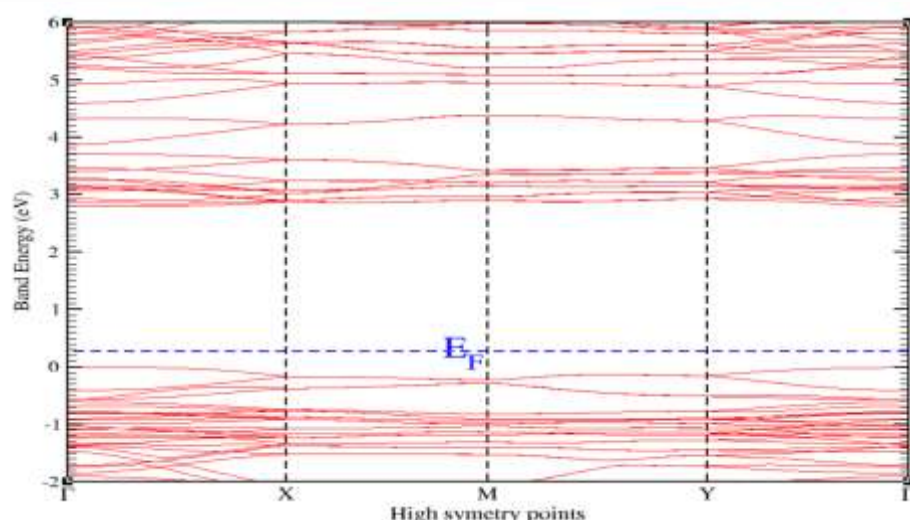
It is observed that DA is a wide-band-gap semiconductor with a direct band gap of 2.7eV which is Comparable to the value of 2.834 according to Jain *et al* (2011) and 2.98 eV for Dimethylammonium iodide stabilized bismuth halide perovskite according to Zhao *et al.* (2021). The values obtained are reasonable since it is known that the DFT usually underestimates the band gap.

4.3.2 Density of States (DOS) and the Projected Density of States (PDOS)

To understand the band gap variation of a material, a study of the density of states (DOS) and the projected density of states (PDOS) is necessary. The DOS and PDOS for DA compound are given in figure 9 and figure 10 below respectively. The Fermi level separates the valence and conduction bands. From the total DOS of Sn, I, N, C and $(CH_3)_2 NH_2 SnI_3$ the position and height of spectral peaks infer that the electronic states of Sn, I, N, C and H are hybridized in both valence and conduction bands in some specific regions. The nature of DOS and PDOS spectra reveals that $DASnI_3$ is a semiconductor.

From the graph of partial density of states (PDOS) figure 9 below, the VBM has major contributions from I-5p and Sn-5s and little hybridization by Sn-5p. On the other hand the CBM is significantly contributed from Sn-5p and I-5p and little I-5s. Therefore the prediction across the bandgap is majorly contributed by iodine and tin *s, p* orbitals which suggest strong hybridization.

Figure 9

Density of States of Dimethylammonium Tin Triiodostanate II Indicating that the Fermi Level is Between the Valence Band and the Conduction Band.
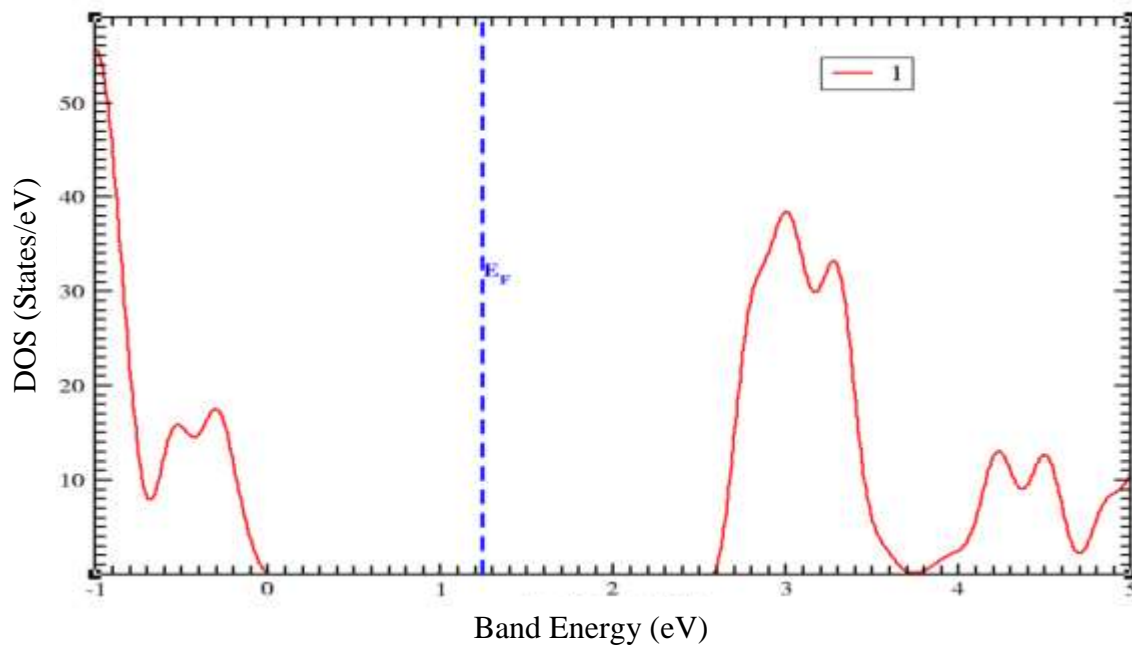
Figure 10

Partial Density of States Obtained for DASnI3 Indicating that Hybridization is mainly Contributed by I and Sn 5p Orbitals.
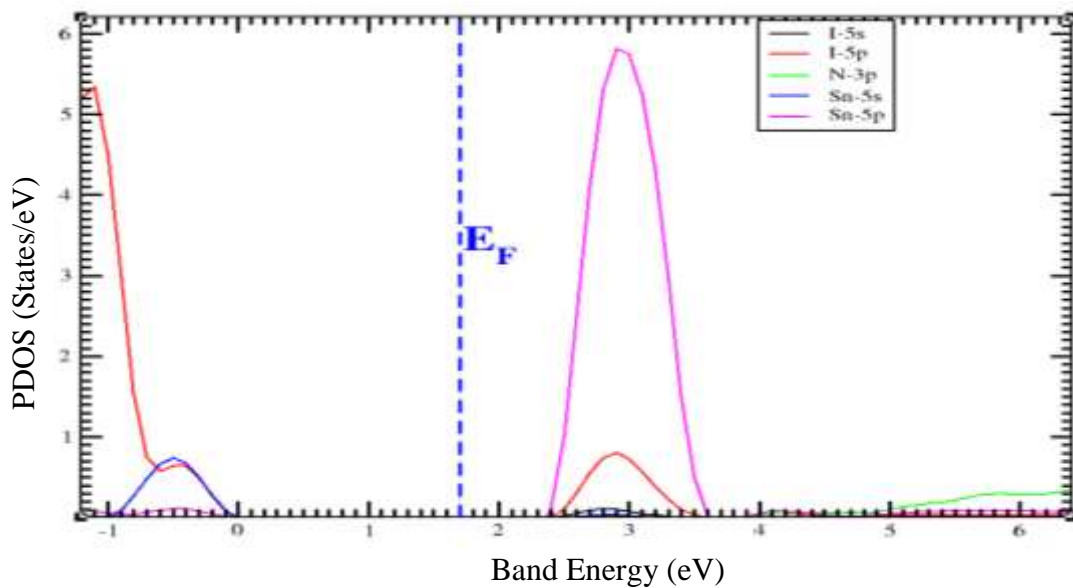
4.4 The Dielectric Constants of Tin Based Perovskites

The optical properties express the interaction of light with the material medium. In this study, the optical properties of Dimethyl ammonium (DA) metal halide perovskites based on the DFT scheme of measuring the different optical parameters was done. To study these properties, the polarization and the absorption of electromagnetic radiation were mathematically presented through the dielectric functions given by the relation below;

$$\varepsilon(\omega) = \varepsilon_1(\omega) + i\varepsilon_2(\omega) \qquad \dots 4.1$$

From the relation above, the first term $\varepsilon(\omega) = \varepsilon_1(\omega)$ represents the real part, showing the polarization of light, the second term is $\varepsilon_2(\omega)$ represents the imaginary part of the dielectric function, and measures the extent on which light is absorbed. The zero frequency limits (static dielectric constant) $\varepsilon_1(0)$ for DASnI3 is 4.0 as shown in table 4 below. This shows that DA has a remarkably large value of $\varepsilon_1(0)$ comparable with that of MAPbI$_6$ with a value of 5.95 its band gap obtained as 1.63 according to srikanth *et al.,* (2020) and EASnI3 with a value of 5.38 having a band gap of 1.17eV according to Joshi *et al.,* (2020). This value reveal that $\varepsilon_1(0)$ increases with the band gap decrease which means that band gap energy is inversely proportional to $\varepsilon_1(0)$. This is consistent with Penn D. (1962) model. From figure 11 below, the maximum value of $\varepsilon_1(\omega)$ is observed to be in the visible energy range (3–3.5 eV) which is equivalent to wavelength of approximately 314-500nm. In the solar spectrum, the visible energy wavelength is from around 380-780nm translating to approximately 1.6-3.5eV. The humps then decreases rapidly followed by small humps which can be caused by the inter-band transitions between valence band and the conduction bands. On the other hand, the imaginary part of the dielectric function is a measure of the extent of light absorption.

It is a basis parameter since all other optical parameters including $\varepsilon_1(\omega)$ are calculated from $\varepsilon_2(\omega)$. In figure 12 below, high absorption peaks are observed in the visible spectral region at energy around 2.5–4.5 eV. Several weak peaks are observed in the energy range of 4.5–14 eV.

Table 4

The Zero-Frequency Values of the Real Part of the Dielectric Function and Band Gaps

Compound	$\varepsilon_0(\omega)$	Bandgaps (eV)	References
C2H8I3N1Sn1	4.0	2.7	This work
MAPbI	6.0	1.7	Wang *et al* 2015
CsPbI3	5.0	1.73	Ahmad *et al* 2017
EASnI3	5.38	1.17	Joshi *et al* 202

Figure 11:

Real Part of the Dielectric against Photon Energy of DASnI3 Highest Peak at 3.3eV
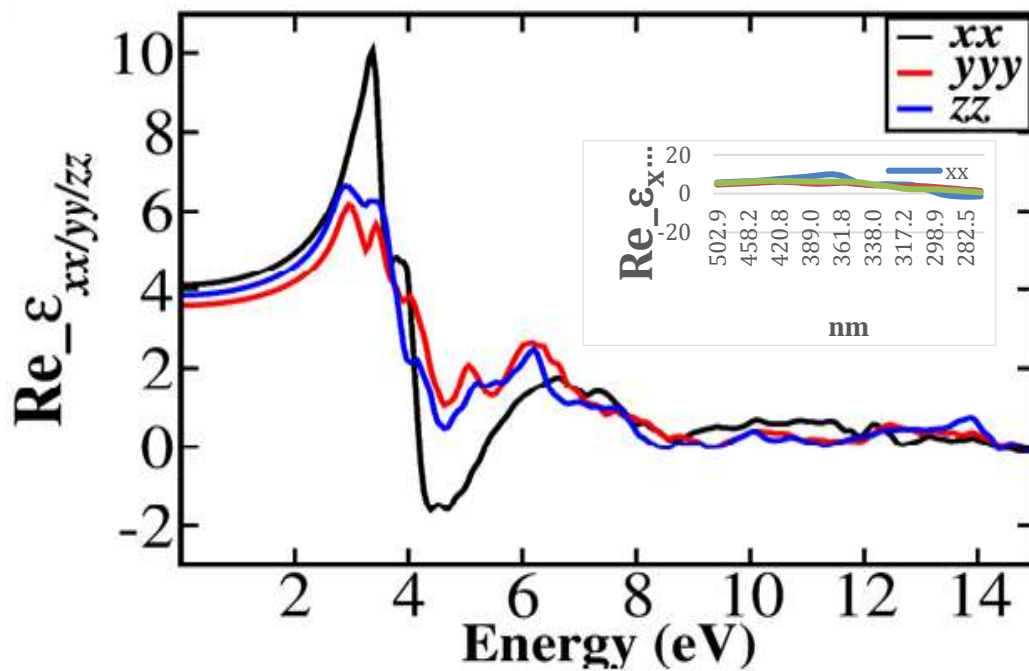
Figure 12:

Imaginary part of the Dielectric Against Photon Energy of Dasni3 Absorbtion Beginning from 2.5eV .
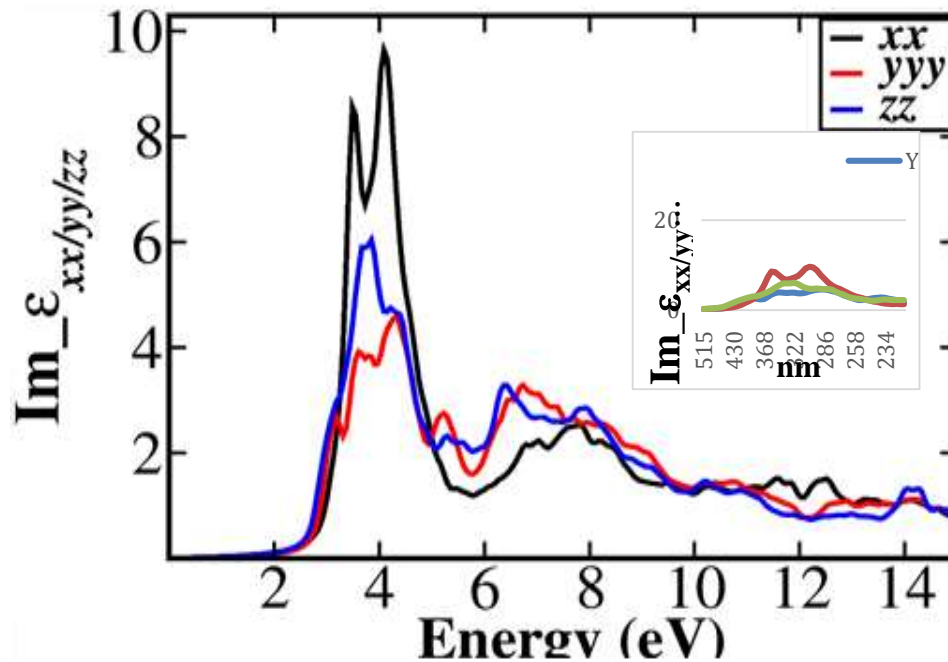
Table 5

Real Part of the Dielectric $\varepsilon_1(\omega)$ and the Imaginary Part $\varepsilon_2(\omega)$ in eV compared with the Values obtained from other Studies.

Dielectric constants	This work	Jain *et al.*, 2011	Saeed *et al.*, 2021
		1.94	3.0
$\varepsilon_1(\omega)$	3.0		
$\varepsilon_2(\omega)$	3.5	2.72	2.5

4.5 Elastic Constants

The structure stability and strength of a material due to an external force, can be determined by studying the elastic constants of a material and which plays an important role in the basic phenomena of solid state including; inter-atomic bonding, phonon spectra, and equation of state. The elastic constants are computed using independent elastic coefficients C_{ij} using the thermo_pw embedded in quantum espresso code.

Shear modulus G gives the information about the rigidity of a material to reversible deformation when under shear stress. Shear modulus thus determines the hardness of a material. The calculated value of G for DASNI3is 6.0251 GPa. A study on Cs2InBiI6 by Saeed *et al.,* 2021 obtained a value of 43.4GPa hence a stiff material, while the value obtained by Feng et al (2014) for MASnI3 was 4.1GPa. This affirms that DASNI3 is a stiff material. Young's modulus (E) determines the toughness of a material thus a reaction of a material towards linear deformation. According to Saeed *et al* (2021), the higher the value of (E) the tougher the material. The value of 1.64518 GPa for DASnI3 indicates that this material is tough.

To examine the ductility/brittleness of a material Pugh's ratio (B/G) is used (Orio *et al* 2009) states that, a material is ductile if B/G value is higher than 1.75 and it is brittle if less. Our calculated results for DASnI3 was 3.27 a much higher value of B/G than the critical value of 1.75.This confirms that the material is ductile in nature.

Poisson's ratio (μ), explains the compressibility of the material which is given by the ratio of adjacent longitudinal strain in non-axial tensile stress. Feng *et al* (2014) states that a material having $\mu > 0.26$ the solid is ductile thus, the larger the Poisson's ratio (μ), the softer the material. This means that when the material is stretched there will be no adjacent reduction of dimensions The Poisson's ratio for DASnI3 is 0.36, indicating that this material is ductile. Decampo *et al.,* (2013) argues that, this could be due to the weak chemical bonds in the perovskite compounds which depends on the constructed elements. The soft characters of the perovskite could therefore be exploited in the tuning of the band gap by strain engineering in application Frost *et al.,* (2014). Anisotropy is defined as the quality of exhibiting properties and gives different values when measured along axes in different directions. The anisotropic parameter (A) for an

ideal isotropic system, is unity and diverges from unity for an anisotropic systems. The universal anisotropy A^U of MASnI3 according to Feng et al., (2014) is 5.23 which vary largely along different orientations. This result indicates that MASnI3 is unstable under ambient conditions. The B/G of 3.26 which is much higher than 1.75 and the poison's ratio of 0.36 obtained above` demonstrates that DASnI3 is a ductile material. The calculated anisotropy of 1.7 showed that DASnI3 was elastically anisotropic since it was found to be greater than unity. The obtained values and those from other works are presented in table 6 below;

Table 6

Calculated Elastic Constants, Bulk modulus (B) in GPa, Young Modulus (E)in GPa and Shear Modulus (G) in GPa, the Poisson's ratio (µ), Anisotropy factor (A), B/G ratio for DASnI3 in Comparison to other Works.

Parameters S_{ij} (1/Mbar)	This work DASnI$_3$	MASnI$_3$ (Feng *et al.*, 2014)	Cs$_2$InBiI$_6$ (Saeed *et al.*, 2021)
C_{11}	23.133	46.1	71
C_{22}	263.79112	21.2	20
C_{33}	-213.46697	16.7	62
C_{55}	83.30059	0.5	-
C_{66}	98.79755	8.3	-
C_{12}	244.16719	12.1	-
C_{13}	-105.73512	26.7	-
C_{23}	287.37204	6.8	-
A	1.7	5.23	2.43
B	19.684144	18.5	37.0
E	16.45108	16.7	
G	6.02501	4.1	99.6
μ	0.36523	0.35	0.05
$\dfrac{B}{G}$	3.267	2.99	0.85

The Debye temperature (D) and the sound velocities in a crystal are closely hinged to the elastic properties. The sound velocity, the Debye temperature and the elastic properties are given by the following equations;

$$\Theta_D = \frac{h}{k}\left[\frac{3n}{4\pi}\left(\frac{N_A\rho}{M}\right)\right]^{1/3}V_m,$$ … 4.2

$$V_m = \left[\frac{1}{3}\left(\frac{2}{V_l^3} + \frac{1}{V_t^3}\right)\right]^{-\frac{1}{3}},$$ … 4.3

$$\left\{V_l = \sqrt{\left(B + \frac{4}{3}G\Big/\rho\right)}\right.$$
$$V_t = \sqrt{G/\rho}$$ … 4.4

Where, h is the Planck constant, k the Boltzmann constant, N_A is the Avogadro's number, n the number of atoms in the molecule, M the molecular weight, and ρ is the density. B and G are bulk and shear moduli, respectively. The transverse (V_t), and the longitudinal (V_l) sound velocities are averaged to give (V_m). Debye temperature and the sound velocities represents the strength of the bond that exist in the structure. The Debye temperature for an orthorhombic MASnI3 is 158K while that of MASnBr3 is 213k (Feng et al., (2014).The size of the organic cation and the hydrogen bonds can affect the octahedron volumes which in turn affects the volume of the unit cell that induces phase transitions. For instance the cubic phase MAPbI3 undergoes a phase transition to Tetragonal at T=327k and a transition to Orthorhomic structure at T=161k (Poglitsch et al., 1987). The use of a larger cation like the DASnI3improves thermal stability through the stronger H-bonds which suppresses ion migration. The Debye temperature value obtained for DASnI3 is 179.165 K while the sound velocity obtained is 1551.193m/s this shows that the Sn-I bonding in this material is strong. The compressional velocity V_P obtained was 2410.521 m/s while the Bulk velocity is V_B is 2362.789 m/s and the Shear velocity V_G is 413.376 m/s

4.6 Photovoltaic Application of Dimethylammonium Triiodostanate II

A direct bandgap material is more efficient for optoelectronic applications when compared with an indirect band gap material because of phonon involvement, which makes indirect band gap semiconductors a bad emitter of light as stated by Khan *et al.,* (2013). From the study of DASnI3, shows that it can be used for photovoltaic application because Dimethyl ammonium can improve both thermal stability and charge transport. Bian *et al.,* (2020) states that when DA is used, it alters the size of the BX6 octahedral affecting the band gap by decreasing the overlap between the metal and the halide orbitals pushing the valence band from the vacuum. A wide band gap material heals deep trap defects resulting in to a more defect tolerant material (Tan et al., 2018).

DOS is mostly used in the study of the physical properties of materials such as the dielectric and the photoemission spectra, and also the transport properties. DOS shows the role and location of different energy orbitals, specifically in the band structure formation. From the total DOS and partial DOS of dimethylammonium tin triiodide, figures 4.5 and 4.6 the high energy in the Sn- 5s states which occupy the VBM are mainly responsible for the promising photovoltaic properties. These states are stable with respect to decomposition (Xiao *et al.,* 2017).

From the study of the imaginary part of the dielectric figure 4.8, there are two characteristic peaks with the energy ranging from 2.5eV – 4.5eV which is within the region of visible light in the solar spectrum. This indicates that DASnI3 readily absorbs photons of energy equivalent to the band gap energy of 2.7eV. The peaks could be attributed to direct inter-band transition of the filled I-5p and Sn-5s VBM states to the unoccupied CBM Sn-5p and I-5p orbitals. The Valence Band Maxima and the Conduction Band Minima of DASNI$_3$ are located at Γ symmetry of the Brillouin zone

and have large band dispersion. This large band dispersion results in the small carrier effective masses.

The value of 3.26707 obtained for B/G which is higher than the critical value of 1.75 indicates that the material would have a deformation and the properties remain subject to bending and even compression. Therefore, from the large B/G ratio of DASnI3 one could use in fabricating thin film absorber working at room temperature. The Poisson's ratio for DASnI3 is 0.36 which is higher than 0.26 a value indexing the ductility of a material, this shows that the material is incompressible and could have a good ductile ability serving as a flexible layer substrate on the polymer. The anisotropy value obtained for DASnI3 is 1.7 it is closer to unity as compared with other materials such as MASnI3 with anisotropy above 5.0. This means that DA cation is nearly isotropic indicating that this material is stable under ambient conditions.

Apart from the size of the A site cation, temperature also induces the polarizability of the material (Srikanth *et al.,* 2021). The lower temperature hexagonal structure of DA exhibits high dielectric constant and this is beneficial as the top layer protecting the active layer of the perovskite. Thus, the orthorhombic DASnI3 perovskite layer can be used as a solar cell material for photovoltaic application.

CHAPTER FIVE

SUMMARY, CONCLUSION AND RECOMMENDATIONS

5.1 Introduction

This chapter presents the summary of the study which was carried out with the aim of using first principles computational modeling implemented in quantum espresso software based on DFT. The conclusion and recommendations on the study of the orthorhombic phase DASnI3 is presented.

5.2 Summary

The main objective of this study was to determine the structural, electronic, dielectric and elastic properties of tin halide perovskite for photovoltaic application. The oxidation state of tin is high, making tin halides unstable under ambient conditions. To exploit the promising properties in photovoltaic application it required identification of an appropriate material that improves the stability and good absorption of the tin halide perovskite based compounds. In this study calculations of the electronic, structural, elastic and dielectric constants of DASnI3 were done and since it was based on DFT, it restricted computations to ground state conditions only.

It was noted that the use of DA as the A site stabilized the perovskite under ambient conditions. Notably, the Anisotropy factor of 1.7 indicates that the material is near Isotropic. It is shown that the results obtained from this study are consistent with other theoretical predictions and experimental values. VBM hybridization was contributed by I-5p and Sn-5s and little by Sn-5p. On the other hand the CBM is contributed by Sn-5p and I-5p and little I-5s.

The Fermi level separates the valence and conduction bands. From the total DOS the DASnI3 displayed the properties of a semiconductor as deduced from the band

structure. From this work the absorption of DASnI3 began from 2.5 a high absorption coefficient which indicates that this material is suitable as a solar cell material.

Lattice constants obtained for DASnI3 are in agreement with experimental and theoretical predictions so far obtained. The Burch Murnaghan third order equation of state gave a bulk modulus of 19.68GPa, which corresponds fairly well with the experimental value of 18.5 GPa for MASnI3. The DASnI3 structure has a wide and direct band gap of 2.7 eV, shear modulus G of 6.0251 GPa was obtained indicated that the material is rigid towards reversible deformation. Young's modulus (E) value of 1.64518 GPa for DASnI3 indicates that this material is tough towards linear deformation. Pugh's ratio (B/G) of 3.26 is higher than 1.75 and the poison's ratio of 0.36 obtained ` demonstrates that DASnI3 is a ductile material.

5.3 Conclusion

The Knowledge of the absorption coefficients, lattice parameters, elastic constants and the band gap of a material helps engineers to design and fabricate a suitable material for solar cells. From this study, the results obtained can be used to guide experimentalists in coming up with a DASnI3 material as a potential high performance solar cell absorber and also a benchmark in developing perovskite solar cells with higher efficiencies and good performance.

5.4 Recommendations

This research on the study of the properties of DASnI3 recommends the following;

1. From the results obtained, DASnI3 is recommended to be tested in optoelectronic devices. This is due to high absorption onset and likely longer resistance time of the material to moisture on the optical properties.

2. DA structure is one of the bigger *A* site structures orthorhombic phase was studied, therefore a study of phase changes is recommended.

3. The study only dealt with theoretical findings on structural, electronic, dielectric and elastic properties of DASnI3.Experimental study of the orthorhombic DASnI3 is recommended.

REFERENCES

Abid, H., Trigui, A., Mlayah, A., Hlil, E. K., & Abid, Y. (2012). Phase transition in organic–inorganic perovskite (C9H19NH3) 2 PbI2Br2 of long-chain alkylammonium. *Results in Physics*, *2*, 71-76.

Aryasetiawan, F. (1992). Self-energy of ferromagnetic nickel in the GW approximation. *Physical Review B*, *46*(20), 13051.

Babayigit, A., Ethirajan, A., Muller, M., & Conings, B. (2016). Toxicity of organometal halide perovskite solar cells. *Nature materials*, *15*(3), 247-251.

Babkin, V. A., & Pristanskov, A. A. (2012). Research of geometrical and electronic structure molecules isopropylcyclopropane by method MNDO. In *Quantum-Chemical Calculations of Molecular Systems as the Basis of Nanotechnologies in Applied Quantum Chemistry* (pp. 147-151).

Bachhuber, F., von Appen, J., Dronskowski, R., Schmidt, P., Nilges, T., Pfitzner, A., &Weihrich, R. (2014). The extended stability range of phosphorus allotropes. *Angewandte Chemie International Edition*, *53*(43), 11629-11633.

Bian, H., Wang, H., Li, Z., Zhou, F., Xu, Y., Zhang, H., ... & Jin, Z. (2020). Unveiling the Effects of Hydrolysis-Derived DMAI/DMAPbIx Intermediate Compound on the Performance of CsPbI3 Solar Cells. *Advanced Science*, *7*(9), 1902868.

Blaha, P., Schwarz, K., Sorantin, P., & Trickey, S. B. (1990). Full-potential, linearized augmented plane wave programs for crystalline systems. *Computer physics communications*, *59*(2), 399-415.

Braun, M., Tuffentsammer, W., Wachtel, H., & Wolf, H. C. (1999). Tailoring of energy levels in lead chloride based layered perovskites and energy transfer between the organic and inorganic planes. *Chemical physics letters*, *303*(1-2), 157-164

Bretschneider, S. A., Weickert, J., Dorman, J. A., & Schmidt-Mende, L. (2014). Research update: physical and electrical characteristics of lead halide perovskites for solar cell applications. *APL Materials*, *2*(4), 155204.

Burgelman, M., Verschraegen, J., Degrave, S., & Nollet, P. (2004). Modeling thin-film PV devices. *Progress in Photovoltaics: Research and Applications*, *12*(2-3), 143-153.

Burschka, J., Pellet, N., Moon, S. J., Humphry-Baker, R., Gao, P., Nazeeruddin, M. K., & Grätzel, M. (2013). Sequential deposition as a route to high-performance perovskite-sensitized solar cells. *Nature*, *499*(7458), 316-319.

Chang, J. A., Im, S. H., Lee, Y. H., Kim, H. J., Lim, C. S., Heo, J. H., & Seok, S. I. (2012). Panchromatic photon-harvesting by hole-conducting materials in inorganic–organic heterojunction sensitized-solar cell through the formation of nanostructured electron channels. *Nano letters*, *12*(4), 1863-1867.

Chen, Q., De Marco, N., Yang, Y. M., Song, T. B., Chen, C. C., Zhao, H., ... & Yang, Y. (2015). Under the spotlight: The organic–inorganic hybrid halide perovskite for optoelectronic applications. *Nano Today*, *10*(3), 355-396.

Chen, Y., Sun, Y., Peng, J., Zhang, W., Su, X., Zheng, K., & Liang, Z. (2017). Tailoring organic cation of 2D air-stable organometal halide perovskites for highly efficient planar solar cells. *Advanced Energy Materials*, *7*(18), 1700162.

Cheng, Z., & Lin, J. (2010). Layered organic–inorganic hybrid perovskites: structure, optical properties, film preparation, patterning and templating engineering. *CrystEngComm*, *12*(10), 2646-2662.

Chiarella, F., Zappettini, A., Ferro, P., Besagni, T., Licci, F., Cassinese, A., & Aruta, C. (2005). Growth and characterization of hybrid (CnH2n+ 1NH3) 2CuCl4 self-assembled films. *Crystal Research and Technology: Journal of Experimental and Industrial Crystallography*, *40*(10-11), 1028-1032.

Ciucivara, A. I. (2007). Density functional studies of magnetic semiconductors and multiferroics Doctoral dissertation.

De Wolf, S., Holovsky, J., Moon, S. J., Löper, P., Niesen, B., Ledinsky, M., & Ballif, C. (2014). Organometallic halide perovskites: sharp optical absorption edge and its relation to photovoltaic performance. *The journal of physical chemistry letters*, *5*(6), 1035-1039.

Dreizler, R. M., & Gross, E. K. U. (1990). Density Functional Theory Springer Verlag.

Eperon, G. E., Stone, K. H., Mundt, L. E., Schloemer, T. H., Habisreutinger, S. N., Dunfield, S. P., ... & Moore, D. T. (2020). The role of dimethylammonium in bandgap modulation for stable halide perovskites. *ACS Energy Letters*, *5*(6), 1856-1864.

Etgar, L., Gao, P., Xue, Z., Peng, Q., Chandiran, A. K., Liu, B., & Grätzel, M. (2012). Mesoscopic CH3NH3PbI3/TiO2 heterojunction solar cells. *Journal of the American Chemical Society*, *134*(42), 17396-17399.

Fan, J., Jia, B., & Gu, M. (2014). Perovskite-based low-cost and high-efficiency hybrid halide solar cells. *Photonics Research*, *2*(5), 111-120.

Feng, J. (2014). Mechanical properties of hybrid organic-inorganic CH3NH3BX3 (B= Sn, Pb; X= Br, I) perovskites for solar cell absorbers. *Apl Materials*, *2*(8), 081801.

Folk, R. L., & Ward, W. C. (1957). Brazos River bar [Texas]; a study in the significance of grain size parameters. *Journal of sedimentary research*, *27*(1), 3-26.

Fraccarollo, A., Canti, L., Marchese, L., & Cossi, M. (2017). First principles study of 2D layered organohalide tin perovskites. *The Journal of chemical physics*, *146*(23), 234703.

Giannelis, E. P. (1996). Polymer layered silicate nanocomposites. *Advanced materials*, *8*(1), 29-35.

Giannouli, M. (2021). Current Status of Emerging PV Technologies: A Comparative Study of Dye-Sensitized, Organic, and Perovskite Solar Cells. *International Journal of Photoenergy*, *2021*.

Giannozzi, P., Baroni, S., Bonini, N., Calandra, M., Car, R., Cavazzoni, C., & Wentzcovitch, R. M. (2009). QUANTUM ESPRESSO: a modular and open-source software project for quantum simulations of materials. *Journal of physics: Condensed matter*, *21*(39), 395502.

Grånäs, O., Vinichenko, D., & Kaxiras, E. (2016). Establishing the limits of efficiency of perovskite solar cells from first principles modeling. *Scientific reports*, *6*(1), 1-6.

Grancini, G.;Roldán-Carmona, C.;Zimmermann, I.;Mosconi, E.; Lee, X.; Martineau, D.; Narbey, S.; Oswald, F.;Angelis, F. D.;Graetzel, M.   2017 One-Year stableperovskite solar cells by 2D/3D interface engineering.NatureCommunications2017,8, 15684

Green, M. A., Emery, K., Hishikawa, Y., Warta, W., Dunlop, E. D., Levi, D. H., & Ho-Baillie, A. W. (2017). Solar cell efficiency tables (version 49). *Progress in photovoltaics: research and applications*, *25*(1), 3-13.

Green, M. A., Ho-Baillie, A., & Snaith, H. J. (2014). The emergence of perovskite solar cells. *Nature photonics*, *8*(7), 506-514.

Hamada, N., Hwang, M., & Freeman, A. J. (1990). Self-energy correction for the energy bands of silicon by the full-potential linearized augmented-plane-wave method: Effect of the valence-band polarization. *Physical Review B*, *41*(6), 3620.

He, C., Han, F., & Zhang, W. (2022). The InSe/g-CN van der Waals hybrid heterojunction as a photocatalyst for water splitting driven by visible light. *Chinese Chemical Letters*, *33*(1), 404-409.

Hohenberg, P., & Kohn, W. (1964). Inhomogeneous electron gas. *Physical review*, *136*(3B), B864.

Ilyasov, V. V., Pham, K. D., Ershov, I. V., Nguyen, C. V., & Hieu, N. N. (2016). Effect of oxygen adsorption on structural and electronic properties of defective surfaces (0 0 1),(1 1 1), and (1 1 0) TiC: Ab initio study. *Computational Materials Science*, *124*, 344-352.

Iskandarov, A. M., & Jo, U. (2012). The theoretical silicon shear strength in a wide temperature range. *Basic Problems. Mat. Sci*, *9*, 89-93.

Jain, A., Hautier, G., Moore, C. J., Ong, S. P., Fischer, C. C., Mueller, T., ... & Ceder, G. (2011). A high-throughput infrastructure for density functional theory calculations. *Computational Materials Science*, *50*(8), 2295-2310.

Jellicoe, T. C., Richter, J. M., Glass, H. F., Tabachnyk, M., Brady, R., Dutton, S. E., & Böhm, M. L. (2016). Synthesis and optical properties of lead-free cesium tin

halide perovskite nanocrystals. *Journal of the American Chemical Society*, *138*(9), 2941-2944.

Joshi, T. K., Sharma, G., & Verma, A. S. (2020). Investigation of structural, electronic, optical and thermoelectric properties of Ethylammonium tin iodide (CH3CH2NH3SnI3): An appropriate hybrid material for photovoltaic application. *Materials Science in Semiconductor Processing*, *115*, 105111.

Kamminga, M. E., Fang, H. H., Filip, M. R., Giustino, F., Baas, J., Blake, G. R., & Palstra, T. T. (2016). Confinement effects in low-dimensional lead iodide perovskite hybrids. *Chemistry of materials*, *28*(13), 4554-4562.

Kanemitsu, Y., & Handa, T. (2018). Photophysics of metal halide perovskites: From materials to devices. *Japanese Journal of Applied Physics*, *57*(9), 090101.

Kim, H. S., Mora-Sero, I., Gonzalez-Pedro, V., Fabregat-Santiago, F., Juarez-Perez, E. J., Park, N. G., & Bisquert, J. (2013). Mechanism of carrier accumulation in perovskite thin-absorber solar cells. *Nature communications*, *4*(1), 1-7.

Ke, W., Spanopoulos, I., Stoumpos, C. C., & Kanatzidis, M. G. (2018). Myths and reality of HPbI 3 in halide perovskite solar cells. *Nature communications*, *9*(1), 1-9.

Khan, I., Ahmad, I., Rahnamaye Aliabad, H. A., & Maqbool, M. (2012). Effect of phase transition on the optoelectronic properties of Zn1− xMgxS. *Journal of Applied Physics*, *112*(7), 073104.

Khan, I., Ahmad, I., Aliabad, H. R., Asadabadi, S. J., Ali, Z., & Maqbool, M. (2013). Conversion of optically isotropic to anisotropic CdSxSe1− x (0⩽ x⩽ 1) alloy with S concentration. *Computational materials science*, *77*, 145-152.

Kohn, W., & Sham, L. J. (1965). Self-consistent equations including exchange and correlation effects. *Physical review*, *140*(4A), A1133.

Kojima, A., Teshima, K., Shirai, Y., Miyasaka, T. (2009) Organometal Halide Perovskites as Visible-Light Sensitizers for Photovoltaic Cells. J. Am. Chem. Soc. 131, 6050−6051.

Kravcova A.N., Guda A.A., Mazalova V.L., Soldatov A.V., Dzhonson R.L.(2011). The electronic structure of titanium nanoclusters analysis by density functional theory. Nanostruktury Matematicheskaya fizika i modelirovanie. 4: 15-22

Lanty, G., Jemli, K., Wei, Y., Leymarie, J., Even, J., Lauret, J. S., & Deleporte, E. (2014). Room-temperature optical tunability and inhomogeneous broadening in 2D-layered organic–inorganic perovskite pseudobinary alloys. *The journal of physical chemistry letters*, *5*(22), 3958-3963.

Lekina, Y., & Shen, Z. X. (2019). Excitonic states and structural stability in two-dimensional hybrid organic-inorganic perovskites. *Journal of Science: Advanced Materials and Devices*, *4*(2), 189-200

Lichtenstein, A. I., Katsnelson, M. I., & Kotliar, G. (2001). Finite-temperature magnetism of transition metals: An ab initio dynamical mean-field theory. *Physical Review Letters*, *87*(6), 067205.

Liechtenstein, A. I., Anisimov, V. I., & Zaanen, J. (1995). Density-functional theory and strong interactions: Orbital ordering in Mott-Hubbard insulators. *Physical Review B*, *52*(8), R5467.

Liu, M., Johnston, M. B., & Snaith, H. J. (2013). Efficient planar heterojunction perovskite solar cells by vapour deposition. *Nature*, *501*(7467), 395-398.

Liu, Y., Wang, K., Xiao, H., Chen, G., Wang, Z., Hu, T., ... & Ma, L. (2020). Theoretical study of the mechanical properties of CrFeCoNiMo x (0.1≤ x≤ 0.3) alloys. *RSC advances*, *10*(24), 14080-14088

Mao, L., Tsai, H., Nie, W., Ma, L., Im, J., Stoumpos, C. C., & Kanatzidis, M. G. (2016). Role of organic counterion in lead-and tin-based two-dimensional semiconducting iodide perovskites and application in planar solar cells. *Chemistry of Materials*, *28*(21), 7781-7792.

Mao, L., Wu, Y., Stoumpos, C. C., Wasielewski, M. R., & Kanatzidis, M. G. (2017). White-light emission and structural distortion in new corrugated two-dimensional lead bromide perovskites. *Journal of the American Chemical Society*, *139*(14), 5210-5215.

Martin, J. C., Ratnaweera, R. J., Kumar, S., Wen, J. R., Kutayiah, A. R., & Sheldon, M. T. (2020). Detailed balance efficiencies for luminescent solar concentrators with aligned semiconductor nanorods: the benefits of anisotropic emission. *Journal of Photonics for Energy*, *10*(2), 025501.

Matsuishi, K., Suzuki, T., Onari, S., Gregoryanz, E., Hemley, R. J., & Mao, H. K. (2001). Excitonic States of Alkylammonium Lead-Iodide Layered Perovskite Semiconductors under Hydrostatic Pressure to 25 GPa. *physica status solidi (b)*, *223*(1), 177-182.

Mejia-Rodriguez, D., Kunitsa, A., Aprà, E., & Govind, N. (2021). Scalable Molecular GW Calculations: Valence and Core Spectra. *arXiv preprint arXiv:2107.10423*.

Merdasa, A., Bag, M., Tian, Y., Källman, E., Dobrovolsky, A., & Scheblykin, I. G. (2016). Super-resolution luminescence microspectroscopy reveals the mechanism of photoinduced degradation in CH3NH3PbI3 perovskite nanocrystals. *The Journal of Physical Chemistry C*, *120*(19), 10711-10719.

Mejia-Rodriguez, D., Kunitsa, A., Aprà, E., & Govind, N. (2021). Scalable Molecular GW Calculations: Valence and Core Spectra. *arXiv preprint arXiv:2107.10423*.

Minemoto, T., & Murata, M. (2014). Device modeling of perovskite solar cells based on structural similarity with thin film inorganic semiconductor solar cells. *Journal of applied physics*, *116*(5), 054505.

Mitzi, D. B., Wang, S., Feild, C. A., Chess, C. A., & Guloy, A. M. (1995). Conducting layered organic-inorganic halides containing< 110>-oriented perovskite sheets. *Science*, *267*(5203), 1473-1476.

Mitzi, D. B. (1999). A layered solution crystal growth technique and the crystal structure of (C6H5C2H4NH3) 2PbCl4. *Journal of Solid State Chemistry*, *145*(2), 694-704.

Mitzi, D. B. (2001). Templating and structural engineering in organic–inorganic perovskites. *Journal of the Chemical Society, Dalton Transactions*, (1), 1-12.

Mitzi, D. B., Feild, C. A., Harrison, W. T. A., & Guloy, A. M. (1994). Conducting tin halides with a layered organic-based perovskite structure. *Nature*, *369*(6480), 467-469.

Niemann, R. G., Kontos, A. G., Palles, D., Kamitsos, E. I., Kaltzoglou, A., Brivio, F., & Cameron, P. J. (2016). Halogen effects on ordering and bonding of CH3NH3+ in CH3NH3PbX3 (X= Cl, Br, I) hybrid perovskites: a vibrational spectroscopic study. *The Journal of Physical Chemistry C*, *120*(5), 2509-2519.

Noel, N. K., Stranks, S. D., Abate, A., Wehrenfennig, C., Guarnera, S., Haghighirad, A. A., & Snaith, H. J. (2014). Lead-free organic–inorganic tin halide perovskites for photovoltaic applications. *Energy & Environmental Science*, *7*(9), 3061-3068.

Novoselov, K. S., Geim, A. K., Morozov, S. V., Jiang, D., Katsnelson, M. I., Grigorieva, I., ... & Firsov, A. (2005). Two-dimensional gas of massless Dirac fermions in graphene. *nature*, *438*(7065), 197-200.

Nyawere, P. W. O., Makau, N. W., & Amolo, G. O. (2014). First-principles calculations of the elastic constants of the cubic, orthorhombic and hexagonal phases of BaF2. *Physica B: Condensed Matter*, *434*, 122-128.

Orio, M., Pantazis, D. A., & Neese, F. (2009). Density functional theory. *Photosynthesis research*, *102*(2), 443-453.

Parr, R. G., & Yang, W. (1989). Density-functional theory of atoms and molecules Oxford Univ. Press.

Paschal, C., Pogrebnoi, A., Pogrebnaya, T., & Seriani, N. (2020). Methylammonium tin iodide perovskite: structural, electronic and thermodynamic properties by a DFT study with different exchange–correlation functionals. *SN Applied Sciences*, *2*(4), 1-9.

Peng, W., Miao, X., Adinolfi, V., Alarousu, E., El Tall, O., Emwas, A. H., ... & Bakr, O. M. (2016). Engineering of CH3NH3PbI3 perovskite crystals by alloying large organic cations for enhanced thermal stability and transport properties. *Angewandte Chemie International Edition*, *55*(36), 10686-10690.

Penn, D. R. (1962). Wave-number-dependent dielectric function of semiconductors. *Physical Review*, *128*(5), 2093.

Philippe, B., Jacobsson, T. J., Correa-Baena, J.-P., Jena, N. K., Banerjee, A., Chakraborty, S., Cappel, U. B., Ahuja, R., Hagfeldt, A., Odelius, M., Rensmo,

H.(2017) Valence Level Character in a Mixed Perovskite Material and Determination of the Valence Band Maximum from Photoelectron Spectroscopy: Variation with Photon Energy. J. Phys. Chem. C 2017, 121, 26655−26666.

Pisanu, A., Speltini, A., Quadrelli, P., Drera, G., Sangaletti, L., & Malavasi, L. (2019). Enhanced air-stability of Sn-based hybrid perovskites induced by dimethylammonium (DMA): synthesis, characterization, aging and hydrogen photogeneration of the MA 1− x DMA x SnBr 3 system. *Journal of Materials Chemistry C*, *7*(23), 7020-7026.

Popov, A., Obukhovsky, A., & Kuznetsov, S. Calculation Method Of Materials Properties On The Basis Of First-Principles Methods (Or Ab Initio) For The Quantum Chemical Modeling Program Package Named Antares. *Journal of Industrial Pollution Control*, *32*(2), 418-423.

Quan, L. N., Rand, B. P., Friend, R. H., Mhaisalkar, S. G., Lee, T. W., & Sargent, E. H. (2019). Perovskites for next-generation optical sources. *Chemical reviews*, *119*(12), 7444-7477.

Quan, L. N., Yuan, M., Comin, R., Voznyy, O., Beauregard, E. M., Hoogland, S., ... & Sargent, E. H. (2016). Ligand-stabilized reduced-dimensionality perovskites. *Journal of the American Chemical Society*, *138*(8), 2649-2655.

Rakitin, M. C., Mirzoev, A. A., & Mirzaev, D. A. (2010). Izmenenie elektronnoy struktury α-zheleza, soderzhashchego vnedrennye atomy vodoroda (Change of electronic structure in iron containing interstitial atoms of hydrogen). *Vestnik YuUrGU. Seriya: Metalurgiya*, (14), 67-71.

Saeed, M., Haq, I. U., Rehman, S. U., Ali, A., Shah, W. A., Ali, Z., ... & Khan, I. (2021). Optoelectronic and elastic properties of metal halides double perovskites Cs 2 InBiX 6 (X= F, Cl, Br, I). *Chinese Optics Letters*, *19*(3), 030004.

Saliba, M., Matsui, T., Seo, J. Y., Domanski, K., Correa-Baena, J. P., Nazeeruddin, M. K., & Grätzel, M. (2016). Cesium-containing triple cation perovskite solar cells: improved stability, reproducibility and high efficiency. *Energy & environmental science*, *9*(6), 1989-1997.

Senanayak, S. P., Yang, B., Thomas, T. H., Giesbrecht, N., Huang, W., Gann, E., & Sirringhaus, H. (2017). Understanding charge transport in lead iodide perovskite thin-film field-effect transistors. *Science advances*, *3*(1), e1601935.

Saparov, B., & Mitzi, D. B. (2016). Organic–inorganic perovskites: structural versatility for functional materials design. *Chemical reviews*, *116*(7), 4558-4596.

Shi, D., Adinolfi, V., Comin, R., Yuan, M., Alarousu, E., Buin, A., ... & Bakr, O. M. (2015). Low trap-state density and long carrier diffusion in organolead trihalide perovskite single crystals. *Science*, *347*(6221), 519-522.

Slater, J. C. (1937). Damped electron waves in crystals. *Physical Review*, *51*(10), 840.

Snaith, H. J. (2013). Perovskites: the emergence of a new era for low-cost, high-efficiency solar cells. *The journal of physical chemistry letters*, *4*(21), 3623-3630.

Srikanth, M., Ozório, M. S., & Da Silva, J. L. (2020). Optical and dielectric properties of lead perovskite and iodoplumbate complexes: an ab initio study. *Physical Chemistry Chemical Physics*, *22*(33), 18423-18434.

Stoumpos, C. C., Cao, D. H., Clark, D. J., Young, J., Rondinelli, J. M., Jang, J. I., & Kanatzidis, M. G. (2016). Ruddlesden–Popper hybrid lead iodide perovskite 2D homologous semiconductors. *Chemistry of Materials*, *28*(8), 2852-2867.

Stoumpos, C. C., Malliakas, C. D., & Kanatzidis, M. G. (2013). Semiconducting tin and lead iodide perovskites with organic cations: phase transitions, high mobilities, and near-infrared photoluminescent properties. *Inorganic chemistry*, *52*(15), 9019-9038.

Stranks, S. D., Eperon, G. E., Grancini, G., Menelaou, C., Alcocer, M. J., Leijtens, T., & Snaith, H. J. (2013). Electron-hole diffusion lengths exceeding 1 micrometer in an organometal trihalide perovskite absorber. *Science*, *342*(6156), 341-344.

Sutherland, B. R., & Sargent, E. H. (2016). Perovskite photonic sources. *Nature Photonics*, *10*(5), 295.

Szotek, Z., Temmerman, W. M., & Winter, H. (1994). Self-interaction corrected, local spin density description of the $\gamma \rightarrow \alpha$ transition in Ce. *Physical review letters*, *72*(8), 1244.

Songvilay, M.; Giles-Donovan, N.; Bari, M.; Ye, Z.-G.;Minns, J. L.; Green, M. A.; Xu, G.; Gehring, P. M.; Schmalzl, K.;Ratcliff, W. D. et al. 2019 Common acoustic phonon lifetimes ininorganic and hybrid lead halide perovskites.Physical ReviewMaterials,3, 093602.4

Tan, H., Che, F., Wei, M., Zhao, Y., Saidaminov, M. I., Todorović, P., ... & Sargent, E. H. (2018). Dipolar cations confer defect tolerance in wide-bandgap metal halide perovskites. *Nature communications*, *9*(1), 1-10.

Travis, W., Glover, E. N. K., Bronstein, H., Scanlon, D. O., & Palgrave, R. G. (2016). On the application of the tolerance factor to inorganic and hybrid halide perovskites: a revised system. *Chemical Science*, *7*(7), 4548-4556.

Vosko, S. H., Wilk, L., & Nusair, M. (1980). Accurate spin-dependent electron liquid correlation energies for local spin density calculations: a critical analysis. *Canadian Journal of physics*, *58*(8), 1200-1211.

Weinberger, P. J. (1990). *Electron scattering theory for ordered and disordered matter*. Clarendon Press.

Wehrenfennig, C., Eperon, G. E., Johnston, M. B., Snaith, H. J., & Herz, L. M. (2014). High charge carrier mobilities and lifetimes in organolead trihalide perovskites. *Advanced materials*, *26*(10), 1584-1589.

White, T. P., Lal, N. N., & Catchpole, K. R. (2013). Tandem solar cells based on high-efficiency c-Si bottom cells: top cell requirements for> 30% efficiency. *IEEE Journal of Photovoltaics*, *4*(1), 208-214.

Wong, J. H., Royapoor, M., & Chan, C. W. (2016). Review of life cycle analyses and embodied energy requirements of single-crystalline and multi-crystalline silicon photovoltaic systems. *Renewable and Sustainable Energy Reviews*, *58*, 608-618.

Wu, T., Liu, X., Luo, X., Lin, X., Cui, D., Wang, Y & Han, L. (2021). Lead-free tin perovskite solar cells. *Joule*, *5*(4), 863-886.

Wu, T., Qin, Z., Wang, Y., Wu, Y., Chen, W., Zhang, S., ... & Han, L. (2021). The main progress of perovskite solar cells in 2020–2021. *Nano-Micro Letters*, *13*(1), 1-18.

Xiao, Z., Du, K. Z., Meng, W., Wang, J., Mitzi, D. B., & Yan, Y. (2017). Intrinsic instability of Cs2In (I) M (III) X6 (M= Bi, Sb; X= halogen) double perovskites: a combined density functional theory and experimental study. *Journal of the American Chemical Society*, *139*(17), 6054-6057.

Yamada, T., Yamada, Y., Nakaike, Y., Wakamiya, A., & Kanemitsu, Y. (2017). Photon emission and reabsorption processes in CH 3 NH 3 PbBr 3 single crystals revealed by time-resolved two-photon-excitation photoluminescence microscopy. *Physical Review Applied*, *7*(1), 014001.

Yi, C., Luo, J., Meloni, S., Boziki, A., Ashari-Astani, N., Grätzel, C., & Grätzel, M. (2016). Entropic stabilization of mixed A-cation ABX3 metal halide perovskites for high performance perovskite solar cells. *Energy & Environmental Science*, *9*(2), 656-662.

Zhao, H., Chordiya, K., Leukkunen, P., Popov, A., Kahaly, M. U., Kordas, K., & Ojala, S. (2021). Dimethylammonium iodide stabilized bismuth halide perovskite photocatalyst for hydrogen evolution. *Nano Research*, *14*(4), 1116-1125Ciucivara, A. I. (2007). Density functional studies of magnetic semiconductors and multiferroics Doctoral dissertation.

Zhou, D., Zhou, T., Tian, Y., Zhu, X., & Tu, Y. (2018). Perovskite-based solar cells: materials, methods, and future perspectives. *Journal of Nanomaterials*, *2018*.

APPENDICES

Appendix I: Input File for Pwscf Code DASnI3 Structure

```
&control
        calculation='scf'
        restart_mode='from_scratch',
        prefix='C2H8I3N1Sn1',
        tstress = .true.
        tprnfor = .true.,
        pseudo_dir = './',
        outdir='./tmp'
/
&system
        ibrav=8,
        celldm(1) = 15.999,
        celldm(2) =1.0855,
        celldm(3) = 1.7684,
        nat=60,
        ntyp=5,
        ecutwfc = 50.0,
        ecutrho = 500.0,
/
&electrons
        diagonalization='david'
        mixing_mode ='plain'
        mixing_beta= 0.5
        conv_thr =1.0d-8
/
&ions
 ion_dynamics = 'damp'
/
!CELL_PARAMETERS hexagonal
```

!6.288797855 0.00000 0.00000

!0.0015427040 6.2287686345 0.00000

!0.1397331762 -0.0003656253 6.3725602886

ATOMIC_SPECIES

Sn 118.71 Sn.upf

 I 126.9 I.upf

 H 1.008 H.upf

 C 12.01 C.upf

 N 14.01 N.upf

ATOMIC_POSITIONS {crystal}

C	0.37545190490266	0.54012727651583	0.65934868138402	! // C
C	0.87545190132362	0.45987272466293	0.34065131660199	! // C
C	0.37545192528208	0.95987289942723	0.15934901024025	! // C
C	0.87545192538974	0.04012710027358	0.84065099155393	! // C
C	0.60030361577420	0.56206452325180	0.34190277106109	! // C
C	0.10030361658456	0.43793547451174	0.65809722788711	! // C
C	0.60030347396000	0.93793580505177	0.84190298011143	! // C
C	0.10030347203678	0.06206419471102	0.15809701806715	! // C
H	0.41684515973192	0.60538484668557	0.60285626342396	! // H
H	0.91684515941576	0.39461515155851	0.39714373766048	! // H
H	0.41684539449205	0.89461556316294	0.10285618981052	! // H
H	0.91684539418351	0.10538443621010	0.89714380979326	! // H
H	0.39278404494513	0.42444821535818	0.64502486256370	! // H
H	0.89278404383979	0.57555178398249	0.35497513658874	! // H
H	0.39278401001270	0.07555152479338	0.14502471294560	! // H
H	0.89278401018377	0.92444847553307	0.85497528676422	! // H
H	0.44077257101034	0.56948386399122	0.71980671296096	! // H
H	0.94077257028960	0.43051613644859	0.28019328753116	! // H
H	0.44077316228172	0.93051624334583	0.21980675918949	! // H
H	0.94077316207309	0.06948375585222	0.78019324138466	! // H
H	0.47618263706704	0.52997104359293	0.33591993068422	! // H

H	0.97618263683506	0.47002895566025	0.66408006904112	! // H
H	0.47618224640651	0.97002879788149	0.83591971757645	! // H
H	0.97618224754668	0.02997120070659	0.16408028219759	! // H
H	0.63014644478772	0.64444689452047	0.29178169951191	! // H
H	0.13014644448678	0.35555310650591	0.70821829960959	! // H
H	0.63014617600407	0.85555328507931	0.79178155876604	! // H
H	0.13014617543023	0.14444671502652	0.20821844051018	! // H
H	0.62510088487699	0.60397447756918	0.40903329304340	! // H
H	0.12510088532211	0.39602552157747	0.59096670537981	! // H
H	0.62510131589184	0.89602613983427	0.90903322119112	! // H
H	0.12510131490996	0.10397385983628	0.09096677766660	! // H
H	0.68569198152325	0.39438892279058	0.26074586317946	! // H
H	0.18569198125533	0.60561107711002	0.73925413670598	! // H
H	0.68569135605787	0.10561070489820	0.76074605167738	! // H
H	0.18569135599965	0.89438929556203	0.23925394730295	! // H
H	0.66512653150481	0.34657728466289	0.36598497321976	! // H
H	0.16512653170211	0.65342271429306	0.63401502677844	! // H
H	0.66512590450758	0.15342270836132	0.86598530083664	! // H
H	0.16512590486717	0.84657729166384	0.13401469843594	! // H
I	0.80048126360355	0.76043627395666	0.58536892922217	! // I
I	0.30048125621083	0.23956372665200	0.41463107188991	! // I
I	0.80048940289647	0.73954308760091	0.08536271324993	! // I
I	0.30048939191257	0.26045691432216	0.91463728787187	! // I
I	0.74960359317409	0.01896040395094	0.33858402006798	! // I
I	0.24960359548250	0.98103959540001	0.66141598031111	! // I
I	0.74960444043795	0.48103983504475	0.83858612319816	! // I
I	0.24960444096257	0.51896016601921	0.16141387489952	! // I
I	0.20778293715890	0.77954239789852	0.40175589898991	! // I
I	0.70778294213709	0.22045760396552	0.59824409921286	! // I
I	0.20777878510268	0.72044510296921	0.90176056011903	! // I
I	0.70777878488553	0.27955489988867	0.09823944262878	! // I

```
N     0.70209575811332   0.43176806133132   0.32598260539439   ! // N
N     0.20209575592070   0.56823194038320   0.67401739806689   ! // N
N     0.70209568161971   0.06823189890388   0.82598251435273   ! // N
N     0.20209568555601   0.93176809952527   0.17401749092960   ! // N
Sn    0.99343097996360   0.00001680951507   0.50124323038100   ! // Sn
Sn    0.49343097980277   0.99998319014836   0.49875676882459   ! // Sn
Sn    0.99342642523809   0.49976458665827   0.00124491622043   ! // Sn
Sn    0.49342642512532   0.50023541340542   0.99875508333083   ! // Sn
!CELL_PARAMETERS (angstrom)
 !  8.46506651440642   0.00000008482821   0.00000006153744
 ! 0.00000010394008   9.18918708361315  -0.00002131242271
  !0.00000015625339  -0.00003467501264  14.97000358871932
K_POINTS {automatic}
4 4 2  0 0 0
```

Appendix II: Input File for Pwscf Code Supercell DASnI3 Structure

```
& control
        calculation='scf'
        restart_mode='from_scratch',
        prefix='C2H8I3N1Sn1$lat',
        tstress = .true.
        tprnfor = .true.,
        pseudo_dir = '/home/pchemaoi/lustre/pseudo',
        outdir='./tmp'
/
 & system
        ibrav=0,
        nat=60,
        ntyp=5,
        ecutwfc = 60, ecutrho = 480
   /
 &electrons
        electron_maxstep= 1000
        diagonalization='david'
        mixing_mode ='plain'
        mixing_beta= 0.4
        conv_thr =1.0d-2
 electron_maxstep=1000
/
&ions
 ion_dynamics='bfgs'
/
&cell
 cell_dynamics='bfgs'

/
```

ATOMIC_SPECIES

Sn 118.71 Sn.upf

I 126.9 I.upf

H 1.008 H.upf

C 12.01 C.upf

N 14.01 N.upf

CELL_PARAMETERS (Angstrom)

6.996457877 0.000000000 0.000000000

0.000000000 12.119839641 0.006312324

0.000000000 0.054893381 11.806064581

ATOMIC_POSITIONS (crystal)

C	0.430528412	0.525858578	0.822575496
C	0.930528408	0.474141424	0.177424502
C	0.373167871	1.086140304	0.301430693
C	0.873167871	-0.086140305	0.698569308
C	0.581880391	0.550245892	0.340010264
C	0.081880392	0.449754106	0.659989735
C	0.582806477	1.039747671	0.882213083
C	0.082806475	-0.039747671	0.117786915
H	0.327936472	0.666564824	0.574844021
H	0.827936472	0.333435174	0.425155980
H	0.620267198	1.010631075	0.091587162
H	1.120267198	-0.010631076	0.908412837
H	0.452609500	0.408539663	0.782260814
H	0.952609499	0.591460336	0.217739185
H	0.376146112	0.098029620	0.202824940
H	0.876146112	0.901970380	0.797175060
H	0.360591229	0.777977452	0.700162829
H	0.860591228	0.222022549	0.299837172
H	0.418830297	0.776093372	0.152646790

H	0.918830297	0.223906627	0.847353211
H	0.638763091	0.428648613	0.334543850
H	1.138763091	0.571351386	0.665456149
H	0.771175381	1.080106500	0.890592106
H	1.271175382	-0.080106501	0.109407894
H	0.651349657	0.620237051	0.265917368
H	0.151349656	0.379762950	0.734082631
H	0.523316325	1.008360520	0.792898444
H	0.023316324	-0.008360520	0.207101555
H	0.387880547	0.560402889	0.347044485
H	-0.112119453	0.439597110	0.652955513
H	0.557706821	0.942707417	0.943946576
H	0.057706820	0.057292583	0.056053423
H	0.778102837	0.417089029	0.219822924
H	0.278102836	0.582910971	0.780177076
H	0.698211279	-0.027970428	0.684131723
H	0.198211279	1.027970428	0.315868276
H	0.581876773	0.208032221	0.367550529
H	0.081876773	0.791967778	0.632449471
H	0.663846345	0.308114158	0.874424991
H	0.163846345	0.691885842	0.125575008
I	0.703166362	0.618250624	0.510351179
I	0.203166354	0.381749376	0.489648822
I	0.810065544	0.793356297	0.058383426
I	0.310065533	0.206643705	0.941616575
I	0.634270234	-0.097439017	0.295853047
I	0.134270236	1.097439017	0.704146953
I	0.724381834	0.662159042	0.776736057
I	0.224381834	0.337840959	0.223263942
I	0.121033822	0.749191700	0.353401222
I	0.621033827	0.250808302	0.646598776

I	0.224547443	0.798610976	0.890343546
I	0.724547442	0.201389026	0.109656457
N	0.770028853	0.233515610	0.380863886
N	0.270028851	0.766484392	0.619136117
N	0.839308728	0.333542835	0.852044116
N	0.339308732	0.666457163	0.147955889
Sn	0.940908647	0.037845163	0.475598332
Sn	0.440908646	0.962154837	0.524401667
Sn	0.978895529	0.483330128	-0.017523632
Sn	0.478895529	0.516669872	1.017523632

K_POINTS {automatic}

5 5 3 0 0 0

Appendix III: Output File for DASnI3 Elastic Constants

Elastic constant   1   1

      strain   stress (kbar)

      -0.0075000000   8.4990342643

      -0.0025000000   10.4826434249

      0.0025000000   9.5609290361

      0.0075000000   8.4207104104

      Polynomial coefficients

      a1= 0.694539391275E-04

      a2= -0.157259851908E-03

      a3= -0.212353532456E+00

Elastic constant   2   1

      strain   stress (kbar)

      -0.0075000000   23.5146068453

      -0.0025000000   22.1087876851

      0.0025000000   20.7277157821

      0.0075000000   19.9055109225

      Polynomial coefficients

      a1= 0.145350382299E-03

      a2= -0.165981512368E-02

      a3= 0.396733004530E-01

Elastic constant   3   1

strain   stress (kbar)
-0.0075000000   12.2167883236
-0.0025000000   14.0396443495
0.0025000000   14.3093701791
0.0075000000   13.8891316471

Polynomial coefficients
a1= 0.973093736967E-04
a2= 0.718772830108E-03
a3= -0.152482494419E+00

Elastic constant   2   2

strain   stress (kbar)
-0.0075000000   23.7833710357
-0.0025000000   22.3762598807
0.0025000000   23.7081914667
0.0075000000   18.9428751160

Polynomial coefficients
a1= 0.158064681418E-03
a2= -0.179321591106E-02
a3= -0.228286187589E+00

Elastic constant   3   2

strain   stress (kbar)

-0.0075000000   17.2359820169

-0.0025000000   16.8095354834

0.0025000000   17.6372325711

0.0075000000   12.1705490390

Polynomial coefficients

a1= 0.119223632095E-03

a2= -0.195351572953E-02

a3= -0.342628404734E+00

Elastic constant   3   3

strain   stress (kbar)

-0.0075000000   10.1666763349

-0.0025000000   13.9968652313

0.0025000000   14.0415982855

0.0075000000   13.7095481154

Polynomial coefficients

a1= 0.970692121715E-04

a2= 0.145111919735E-02

a3= -0.282943308393E+00

Elastic constant   6   6

strain   stress (kbar)
-0.0075000000   -1.4291688401
-0.0025000000   -1.5525341554
0.0025000000   -3.1428703038
0.0075000000   -4.1923085867

Polynomial coefficients
a1= -0.155659007395E-04
a2= -0.134322446692E-02
a3= -0.629531713761E-01

Elastic constant   5   5

strain   stress (kbar)
-0.0075000000   1.3270925199
-0.0025000000   0.5029664457
0.0025000000   -0.6362442095
0.0075000000   -1.0698568526

Polynomial coefficients
a1= -0.618918037751E-06
a2= -0.113253196203E-02
a3= 0.265465679410E-01

Elastic constant   4   4

strain   stress (kbar)

-0.0075000000   0.3446788485

-0.0025000000   0.3358474181

0.0025000000   -0.1181511049

0.0075000000   -0.4156391143

Polynomial coefficients

a1= 0.862575345464E-06

a2= -0.371836634637E-03

a3= -0.196224787076E-01

Elastic constant   6   1

strain   stress (kbar)

-0.0075000000   -1.4746435704

-0.0025000000   -2.1434849090

0.0025000000   -3.9254072107

0.0075000000   -2.9945625666

Polynomial coefficients

a1= -0.213074013990E-04

a2= -0.862197336803E-03

a3= 0.108744461121E+00

Elastic constant   6   2

strain   stress (kbar)
-0.0075000000   -3.3694714058
-0.0025000000   -3.1778812308
0.0025000000   -2.1261220571
0.0075000000   -2.3297181012

Polynomial coefficients
a1= -0.178600424222E-04
a2= 0.567080324388E-03
a3= -0.268642176597E-01

Elastic constant   6   3

strain   stress (kbar)
-0.0075000000   -1.0600587976
-0.0025000000   -3.5959072214
0.0025000000   -1.9011837012
0.0075000000   -2.8239833950

Polynomial coefficients
a1= -0.193695656885E-04
a2= -0.489045097193E-03
a3= 0.109652842371E+00

Elastic constant   5   4

strain   stress (kbar)

-0.0075000000   -0.0638803921

-0.0025000000   0.3666588858

0.0025000000   -0.4287691651

0.0075000000   -0.0603492231

Polynomial coefficients

a1= -0.184716162908E-06

a2= -0.106703953743E-03

a3= -0.422278733844E-02

Elastic constants C_ij (kbar)

i j=   1   2   3   4   5   6

1   23.13372   244.16719 -105.73512   0.00000   0.00000
126.83359

2   244.16719   263.79112   287.37204   0.00000   0.00000   -
83.42038

3 -105.73512   287.37204 -213.46697   0.00000   0.00000
        71.94101

4   0.00000   0.00000   0.00000   27.34952   7.84835
        0.00000

5   0.00000   0.00000   0.00000   7.84835   83.30059
        0.00000

6   126.83359   -83.42038   71.94101   0.00000   0.00000
        98.79755

1 bar = 10^5 Pa; 10 kbar = 1 GPa; 1 atm = 1.01325 bar; 1 Pa = 1 N/m^2

1 Pa = 10 dyn/cm^2; 1 Mbar = 10^11 Pa

1 torr = 1 mm Hg = 1/760 bar = 7.5006 x 10^-3 Pa

Elastic compliances S_ij (1/Mbar)

i j=   1   2   3   4   5   6

1 -196.37274 27.79046 182.71062   0.00000   0.00000
142.51936

2   27.79046   -2.39250 -23.83998 0.00000   0.00000   -
20.33729

3 182.71062 -23.83998 -171.11933   0.00000   0.00000   -
130.08507

4   0.00000   0.00000   0.00000   37.57975   -3.54066
0.00000

5   0.00000   0.00000   0.00000   -3.54066   12.33831
0.00000

6 142.51936 -20.33729 -130.08507   0.00000   0.00000   -
95.28915

1/Mbar = 1/10^{11} Pa; 1 Pa = 1 N/m^2

Voigt approximation:

Bulk modulus B =   102.78512 kbar

Young modulus E =   52.09104 kbar

Shear modulus G =   18.39978 kbar

Poisson Ratio n =   0.41553

Reuss approximation:

Bulk modulus B =   290.89776 kbar

Young modulus E =   -19.18888 kbar

Shear modulus G =   -6.34975 kbar

Poisson Ratio n =   0.51099

Voigt-Reuss-Hill average of the two approximations:

Bulk modulus B = 196.84144 kbar

Young modulus E = 16.45108 kbar

Shear modulus G = 60.2501 kbar

Poisson Ratio n = 0.36523

Voigt-Reuss-Hill average; sound velocities:

Compressional V_P = 2410.521 m/s

Bulk V_B = 2362.789 m/s

Shear V_G = 413.376 m/s

The approximate Debye temperature is 85.480 K

Average Debye sound velocity = 1551.193 m/s

Debye temperature = 179.165 K

++
++++++++++++++++++++++

Computing the thermodynamic properties from elastic constants

Writing on file therm_files/output_therm.dat_debye.g1

++
+++++++++++++++++++++

THERMO_PW : 15h48m CPU 16h 3m WALL

This run was terminated on: 17:18:29 25Mar2022

Appendix IV: Publication, Conferences and Workshops

Publications

1. Perpetua Jelimo Chemaoi, P.W.O Nyawere, C. M. Maghanga(2021) First principles study of Electronic Properties of Dimethyl-ammonium Tin triidostanate (II) Perovskite for Photo-voltaic Application in solar cell DOI:14445/23500301/IJAP-V813P104

Workshops and Conferences

1. 4th October 2021 participated in the Kabarak University International Conference on Basic Sciences and presented a paper on **Computation of Electronic and Structural Properties of Tin halide Perovskites for Photovoltaic Application by first principles.**

2. 2 nd − 3 rd November 2021 presented a paper on **First principles study of Electronic Properties of Dimethyl-ammonium Tin triidostanate (II) Perovskite for Photo-voltaic Application in solar cell**; at MSSEESA Workshop on Materials for Solar Energy Conversion University of Eldoret, School of science.

3. 3rd June 2020 participated in virtual poster session presented a poster on **Electronic structure properties of tin halides perovskites** university of California Merced Electronic Structure Workshop

4. 5th -6th March 2020 attended a workshop on Density Functional Theory and Beyond at the Catholic University of East Africa.

5. 6th -7th June 2019 attended a workshop on Computational physics codes by the Computational and Theoretical Physics (CThep) Masinde Muliro University of Science and Technology.

Appendix V: KUREC Clearance

KABARAK UNIVERSITY RESEARCH ETHICS COMMITTEE

Private Bag - 20157
KABARAK, KENYA
Email: kurec@kabarak.ac.ke

Tel: 254-51-343234/5
Fax: 254-051-343529
www.kabarak.ac.ke

OUR REF: KABU01/KUREC/001/02/06/21

11th June, 2021

Perpetua Jelimo Chemaoi,
Kabarak University,

Dear Perpetua,

SUBJECT: ETHICS REVIEW DECISION

Kabarak University Research Ethics Committee (KUREC) received application for a protocol titled "COMPUTATION OF ORGANIC-INORGANIC TIN HALIDE PEROVSKITE FOR PHOTOVOLTAIC APPLICATION IN SOLAR CELL" on 07th April, 2021. The protocol was reviewed and discussed during a virtual meeting held on 7th June, 2021 at 1000 Hours. The committee considered the application in accordance with the Kabarak University procedures on review of research protocols for ethical clearance and decided as follows:

1. **PROPOSED STUDY SITE**

   Computer simulation project

2. **KUREC DECISION**

   <u>Approved</u> for data collection for a minimum period of ONE year from 11th June, 2021

This approval is subject to the following conditions:

i. The researcher shall obtain a RESEARCH PERMIT from NACOSTI before commencement of data collection & submit a copy to the Kabarak University Institute of Postgraduate Studies (IPGS);
ii. The researcher shall immediately notify KUREC in case of any adjustments to the protocol;
iii. The researcher shall within 7 days of occurrence notify KUREC of any adverse events associated with the conduct of this study;
iv. The researcher shall apply for extension of the study period should the initial 1 year expire before completion of data collection;
v. The researcher shall submit study progress reports to KUREC after every 6 months and a full report at completion of the study/project

Thank you.

Sincerely,

Prof. Jackson Kitetu PhD.
KUREC-Chairman

Cc   Vice Chancellor
        DVC-Academic & Research
        Registrar-Academic & Research
        Director-Research Innovation & Outreach
        Institute of Post Graduate Studies

Appendix VI: NACOSTI Research Permit

REPUBLIC OF KENYA

NATIONAL COMMISSION FOR
SCIENCE, TECHNOLOGY & INNOVATION

Ref No: 110526

Date of Issue: 02/July/2021

RESEARCH LICENSE

This is to Certify that Ms.. Perpetua Jelimo Chemaoi of Kabarak University, has been licensed to conduct research in Nakuru on the topic: COMPUTATION OF ORGANIC-INORGANIC TIN HALIDE PEROVSKITE FOR PHOTOVOLTAIC APPLICATION IN SOLAR CELL for the period ending : 02/July/2022.

License No: **NACOSTI/P/21/11429**

110526

Applicant Identification Number

Director General
NATIONAL COMMISSION FOR
SCIENCE, TECHNOLOGY &
INNOVATION

Verification QR Code

NOTE: This is a computer generated License. To verify the authenticity of this document,
Scan the QR Code using QR scanner application.

Appendix VII: Conference Participation

KABARAK UNIVERSITY

Certificate of Participation

Awarded to

Perpetua Chemaoi

for successfully participating in the Kabarak University
International Research Conference on Basic Sciences held on
12th October 2021 and presented a paper entitled *"Computation of
Electronic and structural Properties of Tin Halide Perovskites for
Photovoltaic Applications by first Principles."*

Conference Theme

The Role of Basic Sciences on National Policies and Global Trends

Prof. Jackson Kitetu
Dean, School of Science
Engineering &Technology

Dr. Moses Thiga
Director Research, Innovation and
Outreach

Appendix VIII: Publication

Original Article

First-principles Study of Electronic Properties of Dimethyl-Ammonium Tin Triidostanate (II) Perovskite for Photo-voltaic Application in Solar Cell

Perpetua Jelimo Chemaoi[1], P.W.O Nyawere[2], C. M. Maghanga[3]

[1,2,3]Postgraduate Student, Department of Physical Sciences, Kabarak University, Kenya

Abstract - Metal-halide perovskites have emerged as a novel and promising photovoltaic materials for use in solar cells. In the current research, they are the potential light-harvesting mediums. The electronic properties of Dimethylammoniumtriodostanate (II) hybrid halide perovskites are of much importance and need to be studied because it can be a good light absorber material due to the wide bandgap exhibited. We employed the PBE-GGA exchange-correlation implemented in Quantum Espresso based on DFT to study the electronic properties. From the study, the band structure and energy bandgap of 2.7 ev a direct bandgap were obtained. The density of states (DOS) and the partial density of states(PDOS) were also determined. It was found that the VBM major contributions are from I-5p and Sn-5s and little hybridization by Sn-5p. On the other hand, the CBM is significantly contributed from Sn-5p and I-5p and is little hybridized by I-5s. The band structure and the density of states (DOS) are important in analyzing the electronic properties of materials which are key in the use of DASNI3 as a solar cell material in photovoltaics.

Keywords — *Density, functional, theory, first, principle*

I. INTRODUCTION

Perovskite materials are potential organic-inorganic materials to be used as photo-absorbers in perovskite-based solar cells. The interesting characteristics of the inorganic components in the hybrid perovskite materials include good thermal stability and a high degree of structural order, according to Fan *et al.* (2014). The organic components are also important due to their functional versatility, their low process-ability cost and mechanical flexibility (Giannelis, 1996). Hence, the possibility of merging the properties of an inorganic crystal and the molecular organic solids has stimulated recent research into the versatile properties of hybrid perovskites, which are organic-inorganic in nature.
The use of Methyl ammonium(MA) as the A site does not

only reduce the formation of defects but incorporating the dipolar MA cation with mixed cation mixed halide will widen the bandgap of the perovskites and also heal deep trap defects resulting in a defect-tolerant material (Tan *et al.*, 2018). An ideal cubic halide perovskite, the B-site, which is the divalent metal, is located at the body-centred position of the cube, and the anions occupy the six face-centred locations forming an octahedral surrounding for the divalent metal, the monovalent cations are situated at the vertices of the cube.
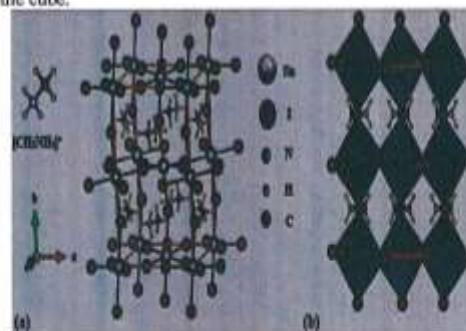

Fig 1: The orthorhombic phase of CH3NH3SnI3 represented as balls and sticks in (a) and polyhedral style (b) adapted from Paschal et al. (2020)

A new choice of *A*-site cation, for instance, Dimethyl Ammonium (DA) which is larger in size than methylammonium (MA), results in an increase in the bandgap (Hautzinger*et al.*, 2020). This is due to the modification of the lattice constant. The extent of the metal-halide orbital overlap is influenced by the A-site cation. Philippe *et al.* (2017) state that this change of the bonding of the metal halide has a direct impact on band positions, the

valence band and the conduction band. For instance, when DA is used as the A-site cation, the bandgap of the perovskite increases as compared with MA perovskite. This fact can be exploited to achieve the most recent advances in photovoltaic performances. This shows that DA produces more thermally stable materials and are also promising materials in reaching higher efficiencies in photovoltaics (Goetzberger et al., 2003). The 3D perovskites exhibits have been proven to exhibit a sharp optical absorption onset, according to De Wolf *et al.* (2014). The physical and chemical properties of any system are affected mainly by the interaction of the electrons with the atomic cores. These are electron-electron interaction, nuclear-electron interaction and nuclear-nuclear interaction. The major source of difficulty in these interactions is the treatment of electron-electron interaction while interpreting their properties since the interactions are inseparable and are only treated with approximation. There are many forms of modelling approaches that are mainly *ab-initio* in nature for the approximation (Giannozzi*et al.*, 2001). Here a well solved Schrödinger equation for a specific system can be differentiable from one to another. The solution of the Schrödinger equation remains a difficult task. The introduction of approximations that are used to reduce the equations to a form that can be solved reduces the degree of accuracy and the predictive power. Using computer simulation and applying the density functional theory (DFT) methods involved in various solving of the Schrödinger equations has had remarkable success in calculations involving electronic and other material properties applicable to several other systems (Mattssonetal 2004). The solution of the single-particle equations for electrons in solids results in energy eigenvalues the band structure. The corresponding eigenfunctions provide insight into the arrangement of the electrons from an energetic and spatial perspective and produce the cohesion between atoms in the solid. (May, V., &Kühn, O. 2008). These results can be useful in several applications. For instance, the band structure of the solid can elucidate the way in which the electrons responds to external perturbations such as the absorption or to the emission of light. The response to light is directly related to the optical and electrical properties of the solid. (Ahmed *et al.*, 2019). In a study of the band structure, for example, one can determine the possible optical excitations that determine the colour, reflectivity, and dielectric response of a solid gong et al. (2018). Other effects include the creation of excitons, that is, the bound pairs of electrons and holes, which are important in determining the optical and electrical properties.

Finally, the band structure can also be used in calculating the total energy of the solid, which helps in determining a variety of properties which includes thermodynamic and as well as mechanical properties.

II. METHODOLOGY

All density functional theory (DFT) calculations were performed using Perdew-Burke-Ernzerhof(PBE) Norm conserving pseudopotentials. The PBE pseudopotentials of Tin, Hydrogen, Carbon, Nitrogen and Iodine ('Sn', 'H', 'C', 'N' and 'I') distributed within the QUANTUM ESPRESSO pseudo library were used for all calculations. The Crystal Information Files were obtained from the Materials Project. The cell shape and atomic positions were relaxed in DFT using the standard PBE version of the GGA electron exchange-correlation functionals were the convergence of the plane wave cut-off (ecutwfc), lattice parameters, as well as the charge density cut-off (ecutrho) with the total energy, was achieved. The density of states function $g(E)$, which defines the number of electronic states per unit volume, per unit energy, for electron energies, was determined as stated by Mejia-Rodriguez *et al.* (2021). The density of state function is important for calculations of effects based on band theory.

III. RESULTS AND DISCUSSION

An orthorhombic phase of C2H8I3Sn1N1 with 60 atoms per cell space group Pna21 was considered. The lattice parameter obtained was a = 15.999Å , b = 17.3669 Å and c = 28.2926 Å . Murnaghan's equation of state was used according to Madsen*et al.* (2016) for volume optimization.

A. The Band Structure

The calculated band structure of the orthorhombic phase C2H8I3N1Sn1 crystal along the high-symmetry lines in the first Brillouin zone is presented in Figs. 2 below. The orthorhombic crystal has a direct band-gap at gamma symmetry points of 2.7eV calculated band gap energy from PBE, GGA exchange-correlation functionals. The Fermi level is located between the valence band maxima and the conduction band minima of the material with the Fermi energy of 2.4ev. The diagram below shows the band structure of the dimethyl ammonium trio do stanate (II), where it is observed that DASnI3 is a wide-band-gap semiconductor with a direct bandgap.
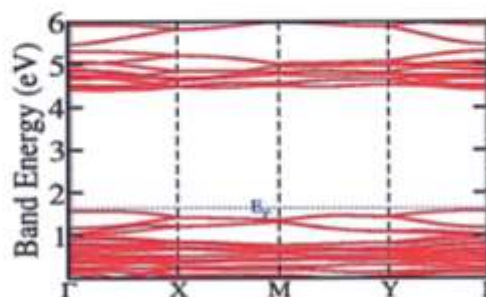

Fig. 2 The band structure of dimethyl ammonium triiodostanate (II)

102

B. The Band Structure

To understand the electronic structure of a material, a study of the DOS and the PDOS is necessary. The DOS and PDOS for DA compounds are given in Figs. 3 and fig 4 below, respectively. The Fermi level separates the valence and conduction bands. From the total DOS of C2H8Sn1N1I3, the position and height of spectral peaks infer that the electronic states of Sn, I, N, C and H are hybridized in both valence and conduction bands in some specific regions. The nature of DOS and PDOS spectra reveal DASnI3 is a semiconductor.

From the PDO's diagram below, the VBM has major contributions from I-5p and Sn-5s and little hybridization by Sn-5p. On the other hand, the CBM is significantly contributed from Sn-5p and I-5p and is little hybridized by I-5s. Therefore the prediction across the bandgap is majorly contributed by iodine and tin s and p orbitals, which suggest strong hybridization.
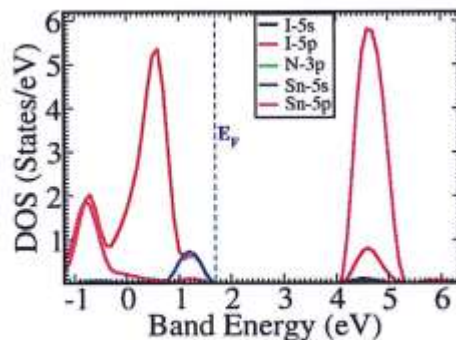

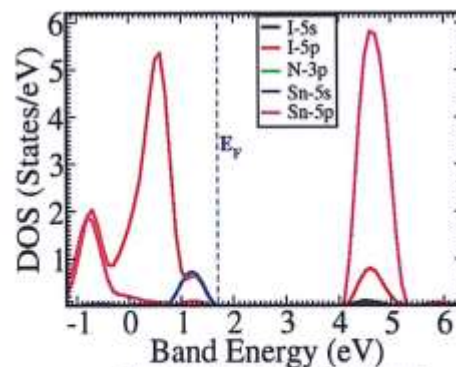**Fig 3. The density of states of Dimethyammoniumtiiodostanate (II)**

Fig 4. Partial density of states of DimethylammoniumTriiodostanate (II)

C. Electronic properties

In order to examine whether a material is an insulator, conductor, or semiconductor, the study of electronic nature through the band structure and density of states (DOS) is important. According to Khan *et al.* (2012), a direct bandgap material is more efficient for optoelectronic applications when compared with an indirect bandgap material because of phonon involvement, which makes indirect bandgap semiconductors a bad emitter of light, as stated by Khan *et al.* (2013)

DOS is mostly used in the study of the physical properties of materials such as the dielectric and the photoemission spectra, and also the transport properties. DOS shows the role and location of different energy orbitals, specifically in the band structure formation. From the total DOS and partial DOS of DASnI3, it is inferred that the high energy in Sn 5s states which occupy the VBM is mainly responsible for the promising photovoltaic properties, according to Xiao *et al.,* 2017. The high energy states observed at the top of the valence band are stable with respect to decomposition. The study of the efficiency of solar cells and other optical materials can be done through observation of the band dispersion and the effective carrier masses. The Valence Band Maxima and the Conduction Band Minima of DASNI3 are located at Γ symmetry of the Brillouin zone and have large band dispersion. This large band dispersion results in the small carrier effective masses.

IV. CONCLUSION

The DASnI3 structure is a wide direct band gap of 2.7 eV material. The Fermi energy is 2.4eV, and it is located between the conduction band and the valence band. The study shows that this material is highly hybridized by the I-5p and Sn-5s. The DASnI3 displayed the properties of a semiconductor as deduced from the band structure. Therefore DASnI3 is a good material to be used in solar cells since it shows that the bandgap was well-modulated and more stable as compared to the traditional MAsnI3 material. It is therefore recommended that an investigation into the cause of the wide bandgap will be insightful.

REFERENCES

[1] Ahmed, N. M., Sabah, F. A., Abdulgafour, H. I., Alsadig, A., Sulieman, A., &Alkhoaryef, M., The effect of post-annealing temperature on the grain size of indium-tin-oxide for optical and electrical properties improvement. Results in Physics, 13 (2019) 102159.

[2] De Wolf, S., Holovsky, J., Moon, S. J., Löper, P., Niesen, B., Ledinsky, M., ...&Ballif, C., Organometallic halide perovskites: sharp optical absorption edge and its relation to photovoltaic performance. The journal of physical chemistry letters, 5(6) (2014) 1035-1039.

[3] Dunfield, S. P., ...& Moore, D. T., The role of dimethylammonium in

bandgap modulation for stable halide perovskites. ACS Energy Letters, 5(6) (2020) 1856-1864

[4] Eperon, G. E., Stone, K. H., Mundt, L. E., Schloemer, T. H., Habisreutinger, S. N., Dunfield, S. P., ... & Moore, D. T., The role of dimethylammonium in bandgap modulation for stable halide perovskites. ACS Energy Letters, 5(6) (2020) 1856-1864

[5] Fan, J., Jia, B., &Gu, M., Perovskite-based low-cost and high-efficiency hybrid halide solar cells. Photonics Research, 2(5) (2014) 111-120.

[6] Giannelis, E. P., Polymer layered silicate nanocomposites. Advanced materials, 8(1) (1996) 29-35.

[7] Giannozzi, P., Baroni, S., Bonini, N., Calandra, M., Car, R., Cavazzoni, C., ...&Wentzcovitch, R. M., QUANTUM ESPRESSO: a modular and open-source software project for quantum simulations of materials. Journal of Physics: Condensed matter, 21(39) (2009) 395502.

[8] Goetzberger, A., Hebling, C., &Schock, H. W., Photovoltaic materials, history, status and outlook. Materials Science and Engineering: R: Reports, 40(1) (2003) 1-46.

[9] Gong, C., Kaplan, A., Benson, Z. A., Baker, D. R., McClure, J. P., Rocha, A. R., &Leite, M. S., Band structure engineering by alloying for photonics. Advanced Optical Materials, 6(17) (2018) 1800218.

[10] Hautzinger, M. P., Pan, D., Pigg, A. K., Fu, Y., Morrow, D. J., Leng, M., &Jin, S., Band edge tuning of two-dimensional Ruddlesden–Popper perovskites by A cation size revealed through nanoplates. ACS Energy Letters, 5(5) (2020) 1430-1437.

[11] Mattsson, A. E., Schultz, P. A., Desjarlais, M. P., Mattsson, T. R., & Leung, K.,Designing meaningful density functional theory calculations in materials science—a primer. Modelling and Simulation in Materials Science and Engineering, 13(1) (2004) R1.

[12] May, V., &Kühn, O., Charge and energy transfer dynamics in molecular systems. John Wiley & Sons., (2008).

[13] Philippe, B., Jacobsson, T. J., Correa-Baena, J.-P., Jena, N. K., Banerjee, A., Chakraborty, S., Cappel, U. B., Ahuja, R., Hagfeldt, A., Odelius, M., Rensmo, H., Valence Level Character in a Mixed Perovskite Material and Determination of the Valence Band Maximum from Photoelectron Spectroscopy: Variation with Photon Energy. J. Phys. Chem. C., 121 (2017) 26655–26666.

[14] Tan, H., Che, F., Wei, M., Zhao, Y., Saidaminov, M. I., Todorović, P., ...& Sargent, E. H.., Dipolar cations confer defect tolerance in wide-bandgap metal halide perovskites. Nature communications, 9(1) (2018) 1-10.

23

104